aer

Atmospheric and
Environmental Research, Inc.

Final Report on

Model Assessment of the Impact on Ozone of Subsonic and Supersonic Aircraft (Contract NAS5-99221)

Prepared by:

Malcolm Ko, Debra Weisenstein, Michael Danilin, Courtney Scott and Run-Lie Shia

Atmospheric and Environmental Research, Inc.
840 Memorial Drive
Cambridge, MA 02139 USA

for

NASA Goddard Space Flight Center
Code 289
Greenbelt Road
Greenbelt, MD 20771

June, 2000

REPORT DOCUMENTATION PAGE

Form Approved
OMB No. 0704-0188

1. AGENCY USE ONLY *(Leave blank)*	2. REPORT DATE	3. REPORT TYPE AND DATES COVERED
	June 19, 2000	Final Report, June 1999 - May 2000

5. FUNDING NUMBERS

NAS5-99221

6. AUTHORS

M. Ko, D. Weisenstein, M. Danilin, C. Scott and R.-L. Shia

7. PERFORMING ORGANIZATION NAME(S) AND ADDRESS(ES)

Atmospheric and Environmental Research, Inc.
840 Memorial Drive
Cambridge, MA 02139

8. PERFORMING ORGANIZATION REPORT NUMBER

P908

9. SPONSORING/MONITORING AGENCY NAME(S) AND ADDRESS(ES)

NASA Goddard Space Flight Center
Code 289
Greenbelt Road
Greenbelt, MD 20771

10. SPONSORING/MONITORING AGENCY REPORT NUMBER

11. SUPPLEMENTARY NOTES

12a. DISTRIBUTION/AVAILABILITY STATEMENT

12b. DISTRIBUTION CODE

13. ABSTRACT *(Maximum 200 words)*

This is the final report for work performed between June 1999 through May 2000 under contract NAS5-99221. The work represents continuation of the previous contract NAS5-32371 which encompasses five areas:

(1) continued refinements and applications of the 2-D chemistry-transport model (CTM) to assess the ozone effects from aircraft operation in the stratosphere;
(2) studying the mechanisms that determine the evolution of the sulfur species in the aircraft plume and how such mechanisms affect the way aircraft sulfur emissions should be introduced into global models;
(3) the development of diagnostics in the AER 3-wave interactive model to assess the importance of the dynamics feedback and zonal asymmetry in model prediction of ozone response to aircraft operation;
(4) the development of a chemistry parameterization scheme in support of the global modeling initiative (GMI);
(5) providing assessment results for preparation of national and international reports.

We participated in the SAGE III Ozone Loss and Validation Experiment (SOLVE) campaign and we continue with our analyses of the data.

Synthetic ozone, high speed civil transport, SOLVE campaign

15. NUMBER OF PAGES
69

16. PRICE CODE

17. SECURITY CLASSIFICATION OF REPORT	18. SECURITY CLASSIFICATION OF THIS PAGE	19. SECURITY CLASSIFICATION OF ABSTRACT	20. LIMITATION OF ABSTRACT
Unclassified	Unclassified	Unclassified	Unlimited

Table of Contents

Abstract

This is the final report for work performed between June 1999 through May 2000 under contract NAS5-99221. The work represents continuation of the previous contract NAS5-32371 which encompasses five areas:

(1) continued refinements and applications of the 2-D chemistry-transport model (CTM) to assess the ozone effects from aircraft operation in the stratosphere;
(2) studying the mechanisms that determine the evolution of the sulfur species in the aircraft plume and how such mechanisms affect the way aircraft sulfur emissions should be introduced into global models;
(3) the development of diagnostics in the AER 3-wave interactive model to assess the importance of the dynamics feedback and zonal asymmetry in model prediction of ozone response to aircraft operation;
(4) the development of a chemistry parameterization scheme in support of the global modeling initiative (GMI);
(5) providing assessment results for preparation of national and international reports which include the "Aviation and the Global Atmosphere" prepared by the Intergovernmental Panel on Climate Change, "Assessment of the effects of high-speed aircraft in the stratosphere: 1998" by NASA, and the "Model and Measurements Intercomparison II" by NASA.

Part of the work carried out under NAS-99221 was reported in the final report for NAS5-32371. (Note that NAS5-32371 ended in February 1998 and the report was written in October 1999. This was done for completeness because many of the reports mentioned in (5) were not finalized until that time. This report is written as an update to the NAS5-32371 report and we will often refer to results reported there.)

We participated in the SAGE III Ozone Loss and Validation Experiment (SOLVE) campaign and we continue with our analyses of the data.

I. Ozone Assessment Calculations Using the AER 2-D CTM

The improvements made to both the chemistry and transport schemes in the AER 2-D CTM were reported in NAS5-32371. The chemistry scheme now includes calculations of effective zonal mean rates for heterogeneous reactions on Polar Stratospheric Cloud taking into account temperature variation along longitudes. The transport scheme simulates the effect of the tropical barrier through adjustment of K_{yy} in the lower stratosphere. A number of refinements were also made to the 2-D aerosol model. The models were used to provide results for the Intergovernmental Panel for Climate Change (IPCC) report (IPCC, 1999), NASA's High Speed Research (HSR) Program report (Kawa et al., 1999), and the Model and Measurement Workshop report (Park et al., 1999).

Debra Weisenstein also took the lead to prepare The IPCC Technical Report, entitled *Model Calculations of the Atmospheric Effects of Supersonic Aviations Which Were Used in the IPCC Special Report on Aviation and the Global Atmosphere.* The report is intended to provide additional detail regarding the supersonic emission scenario calculations presented in Chapter 4 of Penner et al. (1999). Due to the space limitations in the Special Report, detailed plots and discussion for a majority of the model calculations were omitted. The technical report was intended to fill that gap and has been compiled for two reasons: (1) to aid those called upon to review the IPCC Special Report, and (2) to archive and document the calculations performed by nine modeling groups for up to 50 scenarios each. It has been published in electronic form only and may be obtained via ftp download in postscript (.ps) or Adobe Acrobat (.pdf) formats at the following locations:

ftp://typhoon.larc.nasa.gov/pub/Sage/IPCC_TECH_REPORTS/supersonic/report
ftp://ftp.aer.com/IPCC_TECH_REPORT (not for web browsers)
ftp://anonymous@ftp.aer.com/IPCC_TECH_REPORT (for web browsers)

and additionally can be read online via a web browser at:

http://asd-www.larc.nasa.gov/sage/IPCC_TECH_REPORTS/tech.html
http://www.aer.com/groups/chem/ipcc_report/.

II. Intercomparison of AER, GSFC, and LLNL 2-D Models

An intercomparison study was performed between the AER, GSFC, and LLNL 2-D models in which the transport formulations of those models were run within the AER model at their native grid resolutions to simulate the change in ozone in response to a fleet of supersonic aircraft. An inert tracer calculation with source similar to HSCT-emitted NO_y was run to confirm that the transport was implemented properly. Small differences were found between the AER model running the GSFC circulation and the GSFC model itself due to the different transport schemes used (Lin and Rood for GSFC, Smolarkiewicz for AER). It was found that substantial differences between 2-D model results still exist even with identical transport, implying that the difference in chemistry treatments (particularly PSC treatment) is still significant and should be resolved.

III. Modeling Activities Analyzing Microphysical Processes in HSCT Wakes

We developed the AER Far-wake model to simulate the evolution of sulfur species in the far-wake and determine how the background aerosol sulfate layer is affected. Our results showed that the ozone response to a HSCT fleet is sensitive to the SO_3/SO_2 ratio at the nozzle plane and the possibility of heterogeneous conversion of SO_2 to sulfate in the near-field. Changes in sulfate surface area caused by sulfur content in the fuel calculated by the AER model were used by all models in the assessment calculations for the IPCC report and the HSR report.

We cooperated with Drs. B. Kärcher and R. Busen (DLR Institute of Atmospheric Physics, Germany), R.P. Turco and F. Yu (UCLA), and R.C. Miake-Lye (Aerodyne Research, Inc.) in estimating global implications of the available particle samplings in aircraft wakes. The main results of this cooperation are presented in the Kärcher et al. (2000) paper, submitted to Journal of Geophysical Research (see Appendix 1). In this report, we briefly outline our contribution to this study.

A phenomenological model has been developed, which allows estimation of the aerosol size distribution in aircraft wakes based on such given parameters as fuel sulfur content, fraction of emitted sulfur converted to SO_3, emission index of particulate organic matter (POM), wake dilution factor, etc. It was shown that this model could successfully explain existing wake sampling data for both subsonic and supersonic aircraft. However,

this model works only for a relatively young wake (i.e. less than several hours after exhaust). In an old wake, interactions with background aerosol and effects of sulfur photochemistry could be important.

We applied our far-wake (Danilin et al., 1997) and 2-D (Weisenstein et al., 1997) models to estimate effects of the different HSCT emission scenarios on the global sulfate aerosol layer. Our far-wake model was initialized from the phenomenological model for several scenarios and performed calculations up to 2 days. The output of the AER far-wake model (aerosol size distribution and sulfur mass partitioning among SO_2 and H_2SO_4 in gas and liquid phases) is used to initialize the AER 2-D model. The difference between global model runs with and without aircraft sulfur emissions provides the response of the global sulfate aerosol layer. The novel approach used in this study improves the reliability of the previous global studies (e.g., IPCC, 1999), since it constrains them by available wake sampling data.

IV. AER 3-Wave Model

The 3-wave model was used to assess the atmospheric effects of HSCT engine emissions. The results showed that the feedbacks reduce the ozone depletion in northern midlatitudes by 20%, mainly induced by the feedback due to changes in circulation. The reader is referred to the NAS5-32371 for details. There is no new work to report here.

V. Chemistry Parameterization Scheme

We developed a set of polynomials that will calculate the 24-hour averaged production and loss rates of 20 transported species in terms of 18 independent variables. The independent variables are temperature, altitude, latitude, time of the year, sulfate surface area, PSC surface area, and concentrations of species from the 3-D CTM from the previous time-steps. Our test shows that the overall root-mean-square accuracy is about 10% although differences for individual points may be larger. The details were reported in NAS5-32371. This work has been published in JGR in collaboration with Harvard University (Duncan et al., 2000). A copy of the paper is included as Appendix 2.

VI. Modeling Support for the SOLVE Campaign

We used funding from this project to perform model analysis of the possible self-sampling wake measurements by ER-2 during the SAGE III Ozone Loss and Validation Experiment (SOLVE). The SOLVE campaign provided a unique opportunity for in situ measurements of the gas composition and particles in the ER-2 wake under cold conditions in the Arctic lower stratosphere during winter. These measurements could be crucial for our understanding of the projected HCST fleet impact on the atmosphere, since they could provide the necessary constraints for model calculations under PSC-type conditions characterized by non-linear chemistry. To justify the importance of this experiment and demonstrate the possibility of obtaining valuable measurements with the existing ER-2 payload, we performed model calculations for the typical ER-2 exhaust scenario and different ambient conditions. Details of our calculations are shown in Appendix 3. Indeed, we have shown that the ER-2 payload, despite existing limitations of the accuracy and frequency of measurements, could allow us to obtain the necessary information about the ER-2 wake composition.

During the SOLVE campaign, two ER-2 wake interceptions occurred during the flights on January 31 and March 7, 2000. The first event on January 31 was characterized by weak perturbations of CO_2 and H_2O, indicating that measurements were made at the very edge of the ER-2 wake. However, the second event, on March 7, showed a strong increase in NO_y, H_2O, and particle concentrations, signaling that the ER-2 wake was penetrated. Our further efforts will be focused on this event.

According to the SOLVE data exchange protocol, we cannot present these measurements in this report. However, we would like to report that we are working closely with the PIs of the relevant instruments. Also, we cooperate with Drs. R.C. Miake-Lye and R.C. Brown (Aerodyne Research, Inc.), who can provide the necessary input data for our far-wake model calculations. Results of our model analysis will be presented at the SOLVE Science Team Meeting in September 2000.

VII. Various Meetings

VII.1 Meeting on Next Generation Supersonic Civil Transport Risk Assessment Methods, Washington DC, November 1999

This is a workshop organized by EPA and NASA to advise ICF Consulting on their plan to assess the health risks associated with oozne depletion that may arise from aircraft operation. The meeting took place at the Office of *ICF Consulting*, Washington, DC, November 18-19, 1999. Malcolm Ko was invited to the meeting and participated in the preparation of the workshop summary. A second meeting is being scheduled in August 2000.

VII.2 GMI Meeting, Washington DC, January 2000

Malcolm Ko attended the GMI meeting January 2000 and made a presentation on "The possible future roles for 2-D models in GMI". The presentation was made in collaboration with Charles Jackman from GSFC. A copy of the viewgraphs is included in Appendix 4.

VII.3 AESA Meeting, Snowmass CO, June 2000

Debra Weisenstein and Michael Danilin attended the AEAP workshop at Snowmass CO. A GMI meeting was scheduled. Michael Danilin made a presentation entitled "Global Implications of the Ozone Loss in a Space Shuttle Wake". A copy of the viewgraphs is included in Appendix 5.

VIII. List of Publication Supported by NAS5-99221 and NAS5-32371

Rinsland, C.P., M.R. Gunson, M.K.W. Ko, D.K. Weisenstein, R. Zander, M.C. Abrams, A. Goldman, N.D. Sze, and G.K. Yue (1995) H_2SO_4 photolyis: A source of sulfur dioxide in the upper stratosphere. *Geophys. Res. Lett.*, 22, 1109-1112.

Plumb, R. A., M.K.W. Ko, and R.L. Shia (1995) Representation of localized aircraft NO_y emissions in a two-dimensional model of stratospheric ozone. *J. Geophys. Res.*, *100*, 20,901-20,911.

Weisenstein, D.K., M.K.W. Ko, N.D Sze, and J.M. Rodriguez (1996) Potential impact of SO_2 emissions from stratospheric aircraft on ozone. *Geophys. Res. Lett., 23*, 161-164.

Fahey et al. (1996) In situ observations of NO_y, O_3, and the NO_y/O_3 ratio in the lower stratosphere. *Geophys. Res. Lett., 23*, 1653-1656.

Weisenstein, D.K., G.K. Yue, M.K.W. Ko, N-D. Sze, J.M. Rodriguez, C.J. Scott (1997), A two-dimensional model of sulfur species and aerosol. *J. Geophys. Res., 102*, 13,019-13,035.

Danilin, M.Y., J.M. Rodriguez, M.K.W. Ko, D.K. Weisenstein, R.C. Brown, R.C. Miakelye, and M.R. Anderson (1997), Aerosol particle evolution in an aircraft wake: Implications for the HSCT fleet impact on ozone, *J. Geophys. Res., 102*, 21453-21463.

Keim, E.R., M. Lowenstein, J.R. Podolske, D.W. Fahey, R.S. Gao, E.L. Woodbridge, R.C. Wamsley, S.G. Donnelly, L.A. Del Negro, C.D. Nevison, S. Solomon, K.H. Rosenslof, C.J. Scott, M.K.W. Ko, D.Weisensten, and K.R. Chen (1997), Measurements of NO_y-N_2O correlation in the lower stratosphere: latitudinal and seasonal changes and model comparisons, *J. Geophys. Res., 102*, 13,193-13,212.

Weisenstein, D. K., M.K.W. Ko, I.G. Dyominov, G. Pitari, L. Ricciardulli, G. Visconti, and S. Bekki (1998), The effect of sulfur emissions from HSCT aircraft: a 2-D model intercomparison, *J. Geophys. Res., 103*, 1527-1547.

Shia, R-L., M.K.W. Ko, D. K. Weisenstein, C. Scott, and J. Rodriguez, Transport between the tropical and mid-latitude lower stratosphere: Implication for ozone response to HSCT emissions (1998), *J. Geophys. Res., 103*, 25435-25446.

Danilin et al., Aviation fuel tracer simulation: Model intercomparison and implications (1998), *Geophys. Res. Lett., 25*, 3947-3950.

Wamsley, P.R. et al. (1998), Distribution of halon-1211 in the upper troposphere and lower stratosphere and the 1994 total bromine budget, *J. Geophys. Res., 103*, 1513-1526.

Gao et al., (1999), A comparison of observations and model simulations of No_x/NO_y in the lower stratosphere, *Geophys. Res. Lett., 26*, 1153-1156.

Park, J.H., M.K.W. Ko, R.A. Plumb, C.H. Jackman, J.A. Kaye, and K.H. Sage (eds.), (1999) Report of the Models and Measurements II, *NASA Reference Publication*, in press, Washington, DC.

Fahey, D.W. and U. Schumann (1999) Aviation-produced aerosols and cloudiness, Chapter 3 in *Aviation and the Global Atmosphere*, Intergovernmental Panel on Climate Change (IPCC), Cambridge University Press, UK.

Isaksen, I. and C. Jackman (1999) Modeling the chemical composition of the future atmosphere, Chapter 4 in *Aviation and the Global Atmosphere*, Intergovernmental Panel on Climate Change (IPCC), Cambridge University Press, UK.

Weisenstein, D.K, R.S. Eckman and M.K.W. Ko (1999) Model calculations of the atmospheric effects of supersonic aviation which were used in the IPCC Special Report on Aviation and the Global Atmosphere, ftp://ftp.aer.com/IPCC_TECH_REPORT, pp. 528.

Kawa, S.R., et al., (1999) Assessment of the Effects of High-Speed Aircraft in the Stratosphere: 1998, *NASA/TP-1999-209237.*

Duncan, Bryan, D. Portman, I. Bey and C. Spivakovsky, Parametrization of OH for efficient computation in chemical tracer models, J. Geophys. Res., 105, 12259-12262, 2000.

Kärcher, B., R.P. Turco, F. Yu, M.Y. Danilin, D.K. Weisenstein, R.C. Miake-Lye, and R. Busen, On the unification of aircraft ultrafine particle emission data, J. Geophys. Res., submitted, 2000.

References Cited:

Danilin, M.Y. et al., Aerosol particle evolution in an aircraft wake: Implications for the HSCT fleet impact on ozone, J. Geophys. Res., 102, 21,453-21,463, 1997.

Duncan, Bryan, D. Portman, I. Bey and C. Spivakovsky, Parametrization of OH for efficcient computation in chemical tracer models, J. Geophys. Res., 105, 12259-12262, 2000.

IPCC (Intergovernmental Panel on Climate Change), Aviation and the global atmosphere, Cambridge University Press, Penner et al., eds., 374 pp., 1999.

Kärcher, B., R.P. Turco, F. Yu, M.Y. Danilin, D.K. Weisenstein, R.C. Miake-Lye, and R. Busen, On the unification of aircraft ultrafine particle emission data, J. Geophys. Res., submitted, 2000.

Kawa, S.R., J.G. Anderson, S.L. Baughcum, C.A. Brock, W.H. Brune, R.C. Cohen, D.E. Kinneson, P.A. Newman, J.M. Rodriguez, R.S. Stolarski, D. Waugh, S.C. Wofsy, Assessment of the Effects of High-Speed Aircraft in the Stratosphere: 1998. NASA/TP-1999-209237, Goddard Space Flight Center, Greenbelt, MD, June 1999.

Park, J.H., M.K.W. Ko, C.H. Jackman, R.A. Plumb, J.A. Kaye and K.H. Sage, eds., Models and Measurements Intercomparison, II, NASA/TM-1999-209554, September 1999.

Weisenstein, D.K., et al., A two-dimensional model of sulfur species and aerosols, J. Geophys. Res., 102, 13,019-13,035, 1997.

Appendix 1

On the Unification of Aircraft Ultrafine Particle Emission Data

**B. Kärcher, R.P. Turco, F. Yu, M.Y. Danilin,
D.K. Weisenstein, R.C. Miake-Lye and R. Busen**

On the Unification of Aircraft Ultrafine Particle Emission Data

B. Kärcher[1], R.P. Turco[2], F. Yu[2], M.Y. Danilin[3], D.K. Weisenstein[3], R.C. Miake-Lye[4], R. Busen[1]

Abstract

To predict the environmental impacts of future commercial aviation, intensive studies have been launched to measure the properties and effects of aircraft emissions. These observations have revealed an extremely wide variance with respect to the number and sizes of the particles produced in the exhaust plumes. Aircraft aerosol ultimately contributes to the population of cloud-forming nuclei, and may lead to significant global radiative and chemical perturbations. In this paper, recent discoveries are coordinated and unified in the form of a physically consistent plume aerosol model that explains most of the observational variance. Using this new approach, it is now practical to carry out reliable global atmospheric simulations of aircraft effects, as demonstrated by a novel assessment of the perturbation of the stratospheric aerosol layer by a supersonic aircraft fleet.

1. Introduction

Aviation impacts atmospheric aerosols and clouds by emitting copious amounts of small liquid aerosol and soot particles [*Seinfeld*, 1998; *Boucher*, 1999; *International Panel on Climate Change (IPCC)*, 1999]. However, a quantitative assessment of potential effects requires a better understanding of ultrafine (size $< 10\,\mathrm{nm}$) particle formation mechanisms. Besides sulfuric acid (H_2SO_4), charged molecular clusters (chemi-ions) and condensable organic species have been suggested to explain important aspects of the aerosols observed in jet aircraft plumes [*Yu and Turco*, 1997; *Kärcher et al.*, 1998a]. All of these species have now been measured in-situ under cruise conditions [*Curtius et al.*, 1998; *Slemr et al.*, 1998; *Arnold et al.*, 1999].

To integrate such field data with physical theory to create a more useful model for aircraft emissions, a parameterization scheme is derived here that accurately predicts the properties of volatile jet aerosols. The model is consistent with microphysical mechanisms describing the phenomenology seen in aircraft plumes, including processes driven by electrical charge and organic vapors. We show that existing plume particle measurements obtained over a wide range of flight conditions can be unified within the framework of our new parameterization, dramatically reducing the apparent variability in volatile particle emission indices previously inferred from the field data.

The emission model is finally applied to carry out a new global assessment of aircraft impacts on ambient aerosol properties, narrowing considerably the range of projected enhancements in background aerosol surface area densities associated with commercial air traffic. Hence, we can demonstrate that this approach can be employed in future evaluations of atmospheric perturbations caused by aviation.

2. Lessons From Field Observations

In addition to emitting nonvolatile soot particles formed within the engine combustors, subsonic and supersonic jet aircraft generate volatile particles within their near-field exhaust plumes. Models [e.g., *Danilin et al.*, 1998] and observations [e.g., *Hofmann et al.*, 1998] show that the total background aerosol number and surface area densities can be significantly enhanced by aircraft emissions. The resulting tendencies of aircraft sulfate and soot aerosols to influence cirrus clouds and to alter chemical processes are as yet poorly quantified, limiting our ability to assess climate and ozone impacts [*Kärcher*, 1999]. Indeed, in-situ observations of particles in fresh (plume age $t < 1\,\mathrm{hr}$) aircraft plumes show a considerable scatter in the apparent volatile particle emission index, even for a fixed fuel sulfur (S) emission index EI(S) [*IPCC*, 1999; *Anderson et al.*, 1998; *Schröder et al.*, 1998; *Brock et al.*, 2000]. The factors that contribute to this variability have not been indentified.

It had been proposed that new volatile aerosols are composed mainly of aqueous H_2SO_4 [*Hofmann and Rosen*, 1978]. However, some measurements do not support this presumption [*Miake-Lye et al.*, 1998; *Kärcher et al.*, 1998a; *Yu et al.*, 1999; *Brock et al.*, 2000]. Simulation models that include concurrent emissions of condensable organic species resulting from incomplete fuel combustion along with chemi-ions also formed in the combustors can explain recent field observations for various S emission levels [*Kärcher et al.*, 1998a; *Yu et al.*, 1999]. In contrast, models that neglect organic emissions and chemi-ions either fail to explain observations or require H_2SO_4 emissions exceeding values measured in-situ [*Curtius et al.*, 1998] or calculated using chemical kinetic codes [*Lukachko et al.*, 1998; *Tremmel and Schumann*, 1999]. Nevertheless, the emission indices of organic compounds are not yet well established.

3. Unified Representation of Volatile Particle Properties

3.1. Model Description

We have developed a conceptual model to explain observed ultrafine particle emissions that consolidates several new concepts concerning the physico-chemical mechanisms responsible for the nucleation and growth of aviation plume aerosols. With this model, we have carried out sensitivity studies to identify the key parameters governing particle formation. Consistent with field data, we assume that particulate organic matter (POM) and H_2SO_4 initially condense to form both ionized (subscript i) and electrically neutral (subscript n) aerosol modes. This phase of particle formation occurs at plume ages shorter than $0.1\,\mathrm{s}$. The effects of electrical charge on the particle collection kernels lead to a preferential growth of an 'ion' aerosol mode, whereas the neutral mode particles maintain smaller cluster sizes and are not detectable by condensation nuclei counters (CNCs). Scavenging of the neutral clusters by ion mode particles constitutes the major growth mechanism of the latter during the first minutes of plume evolution. Restrict-

ing the analysis to such times allows the interaction of volatile particles with emitted soot and entrained ambient aerosol to be neglected.

The phenomena noted above can be expressed by means of two simplified equations:

$$\mathrm{EI(POM)} + \frac{98}{32}\eta\mathrm{EI(S)} = \frac{\pi}{6}\sum_{k=i,n}\rho_k W_k N_k D_k^3 \quad (1)$$

$$\frac{dN_n}{dt} = -K n_i N_n \,. \quad (2)$$

Equation (1) describes the overall mass conservation between the prescribed emissions of POM and H_2SO_4 (in units of g emitted per kg of fuel burned, where η is the conversion fraction of fuel S ($32\,\mathrm{g\,mol^{-1}}$) to H_2SO_4 ($98\,\mathrm{g\,mol^{-1}}$) molecules at emission) and the particle mass contained in the two volatile modes (ρ and W are the mass density and mass fraction, respectively, of POM or H_2SO_4). Assuming log-normal size distributions, N and D denote the total particle number per kg-fuel and the volume mean diameter, respectively, for each mode. Beyond a timescale of about 0.1 s, N_i is constant and equal to the number of chemi-ion-induced aerosol particles, which is controlled by ion-ion recombination at earlier times [*Yu and Turco*, 1997]. Equation (2) describes the rate of change in the number of neutral clusters, where the coagulation kernel K depends on D_i. A kernel for thermal coagulation in the free molecular regime of the form $K = K_0(D_i/D_{i0})^2$ is used, where $D_{i0} = 1-4\,\mathrm{nm}$ is the initial value (depending on EI(POM) and on η EI(S)) and $K_0 = 1.2\times10^{-9}\,\mathrm{cm^3\,s^{-1}}$ is the appropriate kernel at that plume age. The choice $K \propto D_i^2$ approximates the collection kernel of small neutral clusters by the growing ion mode particles. (*Turco and Yu* [1999] present the analytical solutions of surface-controlled collection of particles in an expanding plume, among other cases, in a more general context.) D_n is assumed to be constant and equal to 1 nm, since the growth rate of the neutral clusters is slower than of the ionized particles. The plume dilution history enters the model through n_i, the number density of ion mode particles per $\mathrm{cm^3}$ of air. In (2), $n_i = CN_i\mathcal{D}(t)$, where the plume dilution factor [*Schumann et al.*, 1998] is taken to be $\mathcal{D} = (t_m/t)^\alpha$ ($t_m = 1\,\mathrm{s}$ and $\alpha = 0.8$) and where $C \simeq 6\times10^{-11}\,\mathrm{kg\text{-}fuel\,cm^{-3}}$ (evaluated at subsonic cruise conditions) depends on the mass density of air.

Equations (1) and (2) can be solved analytically to obtain the temporal evolution of $D_i(t)$. We simplify aerosol thermodynamics and set $\rho = 1.5\,\mathrm{g/cm^3}$ and $W = 0.6$ for both modes. The maximum ion mode volume mean diameter

$$D_i^\infty = \left[\frac{\mathrm{EI(POM)} + \mathrm{EI}(H_2SO_4)}{\pi\rho W N_i/6}\right]^{1/3} \quad (3)$$

is approached within plume ages $t \simeq 10^3$–10^4 s and lies within the range 6–12 nm. Equation (3) follows directly from (1) with $\mathrm{EI}(H_2SO_4) \equiv 98\eta\mathrm{EI(S)}/32$. Differentiating (1) and then substituting from (2) allows the temporal evolution of $D_i(t)$ to be derived in analytical form. In terms of the normalized variables $x = D_i/D_i^\infty$ and $\tau = t/t_m$ we find:

$$\int_{x_0}^{x}\frac{dx}{1-x^3} = \kappa\int_{\tau_0}^{\tau}\frac{d\tau}{\tau^{-\alpha}} \,. \quad (4)$$

Here $\kappa = K_0 N_i C t_m (D_i^\infty/D_{i0})^2/3$ is the single dimensionless parameter governing the solution obtained in the form $\tau(x)$, from which the temporal evolution of $D_i(t)$ can be derived. The left-hand integral is solved by the method of partial fractions, yielding $F(x) - F(x_0)$, with $F(x) = (1/6)\ln[(1+x+x^2)/(1-x)^2] + (1/\sqrt{3})\arctan[(1+2x)/\sqrt{3}]$. The right-hand integral yields $(\tau^{1-\alpha} - \tau_0^{1-\alpha})/(1-\alpha)$ for $\alpha \neq 1$ or $\ln(\tau/\tau_0)$ for $\alpha = 1$.

To facilitate comparison with observations, we define the apparent particle emission indices, AEIs, as the cumulative number of particles per kg-fuel that are larger than a given size. Hence, the AEI is the convolution of the size distribution of the ion mode particles inferred from (4), after the detection efficiency of the CNC has been taken into account. Although great effort has been spent in calibrating CNCs in the laboratory [e.g., *Cofer et al.*, 1997; *Schröder et al.*, 1998; *Brock et al.*, 2000], their performance under flight conditions remains poorly defined. To incorporate the effects of variable CNC detection efficiencies, ϵ, to a first order and to permit an analytical evaluation, we assume a linear response function

$$\epsilon(D, D_{th}) = 0.5 + \frac{D - D_{th}}{\delta} \,, \quad (5)$$

where δ is the width of ϵ, that is, $\epsilon = 0$ for $D < D_{th} - \delta/2$ and $\epsilon = 1$ for $D > D_{th} + \delta/2$. We use $\delta \simeq D_{th}$ as a free parameter. To obtain the apparent emission indices AEI, we integrate ϵ over the log-normal size spectrum $F(D, D_i^N, \sigma)$, corresponding to the ion mode particles, assuming a modal width $\sigma = 1.3$ and using the mean number diameter $D_i^N(t) = D_i(t)\exp(-3\ln^2\sigma)$ deduced from our analytic solution:

$$\mathrm{AEI}(t) = N_i\int_0^\infty dD\, F(D, D_i^N, \sigma)\epsilon(D, D_{th}) \,. \quad (6)$$

The choice of log-normal size distributions with $\sigma = 1.3$ is supported by a detailed comparison of numerical simulations with near-field data [*Kärcher et al.*, 1998a; *Yu et al.*, 1999].

3.2. Discussion of Model Features

Figure 1 illustrates the behavior of the calculated AEIs as a function of $EI(H_2SO_4) \propto \eta EI(S)$, for various plume ages (1a), POM EIs (1b), and lower CNC detection limits (1c). Common to all of the results in Figure 1 is the decreasing sensitivity of AEI for H_2SO_4 levels above 50–100 mg/kg fuel (or ~ 0.3–0.6 g S/kg-fuel using $\eta = 0.05$; the global average S content is in the range 0.4–0.6 g S/kg-fuel). In Figure 1a, the rapid increases of AEIs at smaller H_2SO_4 levels are caused by the growth of ultrafine particles across the detection threshold D_{th} over the course of time. In contrast, for high H_2SO_4 levels, growth takes place at earlier stages ($t < 1$ s), so that almost all of the ion mode particles (2×10^{17}/kg-fuel in this case) are detected at the plume ages indicated. Since AEIs at even lower $EI(H_2SO_4)$ are determined by the condensation of organics, the AEIs are very sensitive to EI(POM) in this parameter region (Figure 1b). The impact of CNC cut-off sizes is illustrated in Figure 1c. In the near-field plume, the use of instruments with relatively large cut-off diameters ($D_{th} > 5$ nm), like those employed in the earliest plume measurements, virtually precludes the detection of new plume aerosols, although the strong sensitivity of AEI on D_{th} decreases with increasing $EI(H_2SO_4)$ (Figure 1c) and plume age (not shown). The behavior of AEIs indicated in Figure 1 is supported by detailed numerical simulations of plume microphysical processes [*Yu and Turco*, 1997; *Kärcher et al.*, 1998b; *Yu et al.*, 1999], which increases our confidence in the present representation.

In comparing the predictions of (1) and (2) with CNC data from recent in-situ measurements [*Anderson et al.*, 1998, 1999; *Schröder et al.*, 1998, 2000; *Petzold et al.*, 1999], it is noteworthy that the key parameters have quite different ranges of variability. For example, POM emissions are not well characterized observationally while η exhibits a range of 0.005–0.15 and $N_i = (1$–$4) \times 10^{17}$/kg-fuel. Thus, EI(POM) introduces the largest uncertainty into our model, but only at low H_2SO_4 emissions.

3.3. Comparison With Field Observations

Figure 2 depicts the dependence on plume age of observed (symbols) and modeled (curves) AEIs, for the ATTAS aircraft in Figure 2a and for the F-16 aircraft in Figure 2b. While the subsonic ATTAS uses old-technology jet engines, the F-16 is a military airplane capable of supersonic flight and equipped with low-bypass turbofan engines. The F-16 engine combustor and turbine are similar to commercial high-bypass engines and should be representative of recent commercial technology. In Figure 2a, each symbol actually represents an average over many individual observations, with an associated spread in AEI of 30–50% [*Schröder et al.*, 1998]. In Figure 2b, a subset of data points [*Anderson et al.*, 1999] is used, including the non-volatile soot emissions. All of the data points include variations related to differences in engine power settings, the location of the measurement within the plume cross section, and ambient conditions (pressures of 220–360 hPa, temperatures of 220–245 K, and relative humidities of 20–80%). Figure 2 demonstrates the ability of the phenomenological model to explain the near-field observations within the uncertainties of the measurements through the selection of reasonable values for EI(POM), η, and N_i.

The model reflects the generally observed increase in AEIs with rising EI(S). A central conclusion from this work is that much of the scatter in AEIs noted in field measurements can be explained consistently by variations of t, EI(POM), and D_{th}. The seemingly pronounced sensitivities noted earlier are due mainly to the steepness of the large-size tail of the ultrafine particle spectrum. The sensitivity of AEIs to other parameters such as the plume dilution rate and ambient conditions is much less pronounced. This does not hold when contrails form, because water and ice condensation dramatically change the size distributions of the plume particles. Due to the large available surface area of contrail ice crystals, the number of ultrafine particles decreases by coagulation scavenging, even in short-lived contrails [*Anderson et al.*, 1998; *Schröder et al.*, 1998; *Kärcher et al.*, 1998b]. These contrail processing effects are not included in the present model.

4. Unifying Plume Particle Measurements

The data discussed above are replotted in Figure 3a together with measurements obtained in other field missions. Multiple data points for a specific aircraft at a given EI(S) correspond to different plume ages and CNC cut-off sizes. To arrive at a more unified

data set, each point was fitted to the model discussed in Section 3.1, obtaining curves similar to those shown in Figure 2. Then, each AEI was recalculated using a common cut-off size (5 nm) and POM emission index (20 mg/kg-fuel) at a specific plume age (3 s). According to Figure 1, these parameters lead to the largest sensitivity in AEI. The resulting normalized data set is shown in Figure 3b (symbols). We overlay solution curves corresponding to the same t, D_{th}, and EI(POM) at fixed values of η and N_i. These comparisons delineate the common trends that underly the various measurements made behind different aircraft, at different plume ages, and under quite different experimental conditions. Given the spread between the individual data points (vertical bars in Figure 3a), Figure 3b demonstrates that a very wide range of observations can be quantitatively explained using a rather simple conceptual model with only three basic parameters.

The principle trend of the normalized AEIs with EI(S) can be understood even with a constant S conversion fraction η within the range 0.005–0.05, implying that η varies much less than previously conjectured between different types of aircraft [*IPCC*, 1999]. However, for the low-S cases, uncertainties in the choice of EI(POM) do not allow us to draw a definitive conclusion on this point.

We note two exceptions. Assuming $\eta = 0.15$ as perhaps an upper bound, we require a comparatively high value of 70 mg POM/kg-fuel to explain the Concorde data, which were performed in much more aged plumes (15 min–1 hr), exhibiting a much larger spread in AEI [*Fahey et al.*, 1995]. While these values still fall within the ranges reported in the literature [*Climatic Impact Assessment Program (CIAP)*, 1973; *Fahey et al.*, 1995; *Lukachko et al.*, 1998; *Tremmel and Schumann*, 1999], this case deserves specific attention in the future. To explain the F-16 data, we assumed negligible organic emissions and low S conversion (see Figure 2b). Whether this indicates the potential for a substantial variability in the organic emissions, or merely reflects a specific feature of this type of engine and the fuel used, remains open at this time. It should be remarked that discrepancies in the determination of EI(S) for the F-16 have been reported [*Anderson et al.*, 1999]: the cause for the discrepancy between the value of 0.146 g S/kg-fuel used here and 0.018 g S/kg-fuel resulting from two independent laboratory analyses is unresolved.

5. Global Impact of Aviation Particulates on Stratospheric Aerosols

The evaluation of aviation-produced aerosol impacts on the global atmosphere requires the use of a global-scale tracer model in conjunction with a sufficiently detailed characterization of the aircraft emissions. To achieve this goal, we have coupled our analytical formulation for the near-field plume to a far-field plume model [*Danilin et al.*, 1997] and a two-dimensional (2-D) global aerosol model [*Weisenstein et al.*, 1997].

The approach used here combines aerosol formation in the near-field plume, aerosol processing in the far-field plume, and the resulting fleet aerosol source and interaction of aerosol processes with atmospheric dynamics on the global scale. Our parameterization scheme provides unified aerosol size distributions prescribed according to EI(S), EI(POM), and η at plume ages $10^3 - 10^4$ s, excluding the more extreme F-16 and Concorde cases. The far-field model continues the chemical and microphysical processing of the exhaust products within the region of greatest aircraft fuel burn in the Northern Hemisphere (pressure of 65 hPa, temperature of 220 K) for two days as the plume expands. The partitioning of S between aerosols and gas phase species and the size distribution generated after two days are used along with the projected aircraft fuel usage for the year 2015 [*IPCC*, 1999] to obtain the aircraft emission source function for the 2-D simulations, which assume surface sources of S only for the calculation of the background aerosol layer. The far field and global models employ the same aerosol microphysics to track the aerosol evolution. In those models, POM is not dealt with explicitly; instead the mass of emitted POM is incorporated into the aerosols assuming the same properties as H_2SO_4. This assumption is reasonable, because POM is likely to be very soluble in aqueous H_2SO_4 and may also react with the acid to form stable compounds [*Kärcher et al.*, 1998; *Yu et al.*, 1999].

Figure 4 gives the predicted changes of the ambient sulfate aerosol surface area density (SAD) due to the operation of a supersonic aircraft fleet for the region of maximum perturbation as a function of η at emission. The simulations assume 0.4 g S/kg-fuel and either 0, 20, or 60 mg POM/kg-fuel. The results show considerable sensitivity to η, with ΔSAD varying from 0.5–0.8 $\mu m^2\,cm^{-3}$. The changes in SAD should be compared with the simulated background SAD of 0.9 $\mu m^2\,cm^{-3}$. In the stratosphere, ΔSAD in-

creases with rising η because the plume particles become larger and are therefore less efficiently scavenged by background particles. Varying η from 0.005 to 0.1 implies values of 6 to 120 mg H_2SO_4/kg-fuel, which explains the low sensitivity of the results to EI(POM) and its decreasing impact when η rises. Reductions of EI(S) or increases of EI(POM) would lead to a greater influence of the POM emissions. The present simulations are compared with those adopted by the IPCC (diamond in Figure 4), which were based on the same 2-D model but neglected plume processing of the aerosols. The resulting ΔSAD is close to, but slightly larger than, the values plotted for the current case, implying that the IPCC calculations are fairly consistent with the results derived here. The IPCC supersonic scenarios also used higher values of η (0.5, 1) for a sensitivity analysis inasmuch as earlier studies had not precluded such a range.

The present analysis indicates that the most important parameters affecting large-scale cloud and chemical impacts are η and EI(POM). The reduction of both of these factors reduces the particle size and thus their atmospheric residence time. Accordingly, as technological measures are taken to reduce the sulfur in aviation fuel, the importance of POM will increase, leading to the need for better information on POM emissions, speciation, and heterogeneous chemical reactions.

6. Summary and Conclusion

We have developed a unique unified representation of the properties of volatile particles emitted by jet aircraft. Our new parameterization is based upon detailed microphysical mechanisms that incorporate the latest phenomenology observed in aircraft plumes, including the roles of chemi-ions and organic vapors. The main findings of this study are:

1. The scatter in emission indices of volatile particles seen in the field measurements is due mainly to variations of plume age, condensable organic emissions (when low S fuel has been used), and the detection threshold size of the ultrafine particle counters.
2. The principle trend of the volatile particle concentrations with fuel S content can be explained with conversion fractions of S to H_2SO_4 at emission within the range 0.005 to 0.05, implying that S conversion varies much less than previously thought.
3. The key parameters affecting the large-scale cloud and chemical impact of aviation particulates are the S-to-H_2SO_4 conversion fraction and condensable organic emissions, the latter especially below H_2SO_4 emissions of 50–100 mg/kg-fuel.

Here, the model has been extensively compared with a diverse set of measurements taken in jet plumes, and shown to reproduce quite accurately the aerosol properties crucial to environmental assessments. Remarkably, the complex evolution of the particulates can be forecast using only three parameters associated with aircraft engines: the amount of emitted chemiions, sulfuric acid, and condensable organic species. We have given uncertainty ranges of these parameters, within which existing field data can consistently be explained with our approach. While chemi-ion and sulfuric acid emissions are constrained by field data, the a priori unknown speciation and emission levels of organic species introduce the largest uncertainties, but only at low H_2SO_4 emissions.

We have also demonstrated, within the context of a global tracer model, that our unified approach is useful in carrying out detailed simulations of the atmospheric impacts of aircraft fleet operations. Accordingly, we have updated and validated the calculations used in the preliminary IPCC assessment of aircraft effects on climate, and set the stage for future research activities.

Acknowledgments. We are grateful Bruce Anderson (NASA), Chuck Brock (NOAA), and Franz Schröder (DLR) for discussions and data exchange. We wish to thank to David Fahey (NOAA) and Ulrich Schumann (DLR) for constructive comments on the manuscript. This work was facilitated by a NATO Collaborative Research Grant SA.5-2-05 (CRG.971624). R. T. acknowledges support from NASA grant NAG5-2723 and NSF grant ATM-96-18425. M. D. and D. W. are supported by NASA grant NAS5-99221.

References

Anderson, B.E., W.R. Cofer III, J.W. Barrick, D.R. Bagwell, and C.H. Hudgins, Airborne observations of aircraft aerosol emissions, II: Factors controlling volatile particle production, *Geophys. Res. Lett.*, *25*, 1693–1696, 1998.

Anderson, B.E., W.R. Cofer III, and D.S. McDougal, Air Force F-16 Aircraft Engine Aerosol Emissions Under Cruise Altitude Conditions, *NASA TM-1999-209102*. National Aeronautics and Space Administration, 1999.

Arnold, F., J. Curtius, B. Sierau, V. Bürger, R. Busen, and U. Schumann, Detection of massive negative chemiions in the exhaust plume of a jet aircraft in flight, *Geophys. Res. Lett.*, *26*, 1577–1580, 1999.

Brock, C.A., F.P. Schröder, B. Kärcher, A. Petzold, R.

Busen, M. Fiebig, and J.C. Wilson, Ultrafine particle size distributions measured in aircraft exhaust plumes in flight, *J. Geophys. Res.*, submitted manuscript, 2000.

Brown, R.C., M.R. Anderson, R.C. Miake-Lye, C.E. Kolb, A.A. Sorokin, and Y.I. Buriko, Aircraft exhaust sulfur emissions, *Geophys. Res. Lett., 23*, 3603–3606, 1996.

Boucher, O., Influence of air traffic on cirrus occurrence, *Nature, 397*, 30–31, 1999.

Climatic Impact Assessment Program (CIAP), Proceedings of the Second Conference on the Climatic Impact Assessment Program, U.S. Department of Transportation, DOT-TSC-OST-73-4, 173–179, 1973.

Cofer III, W.R., B.E. Anderson, E.L. Winstead, and D.R. Bagwell, Calibration and demonstration of a condensation nuclei counting system for airborne measurements of aircraft exhausted particles, *Atmos. Environ., 32*, 169–177, 1997.

Curtius, J., B. Sierau, F. Arnold, R. Baumann, R. Busen, P. Schulte, and U. Schumann, First direct sulfuric acid detection in the exhaust plume of a jet aircraft in flight, *Geophys. Res. Lett., 25*, 923–926, 1998.

Danilin, M.Y., M. Rodriguez, M.K.W. Ko, D.K. Weisenstein, R.C. Brown, R.C. Miake-Lye, and M.R. Anderson, Aerosol particle evolution in an aircraft wake: Implications for the HSCT fleet impact on ozone, *J. Geophys. Res., 102*, 21,453–21,463, 1997.

Danilin, M.Y. et al., Aviation fuel tracer simulations: Model intercomparison and implications, *Geophys. Res. Lett., 25*, 3947–3950, 1998.

Fahey, D.W. et al., Emission measurements of the Concorde supersonic aircraft in the lower stratosphere, *Science, 270*, 70–74, 1995.

Hofmann, D.J., and J.M. Rosen, Balloon observations of a particle layer injected by stratospheric aircraft at 23 km, *Geophys. Res. Lett., 5*, 511–514, 1978.

Hofmann, D.J., R. Stone, M. Wood, T. Deshler, and J. Harris, An analysis of 25 years of balloon-borne aerosol data in search of a signature of the commercial subsonic aircraft fleet, *Geophys. Res. Lett., 25*, 2433–2436, 1998.

Intergovernmental Panel on Climate Change (IPCC), Aviation and the Global Atmosphere, Special Report, Cambridge Univ. Press, 65–120, 1999.

Kärcher, B., F. Yu, F.P. Schröder, and R.P. Turco, Ultrafine aerosol particles in aircraft plumes: Analysis of growth mechanisms, *Geophys. Res. Lett., 25*, 2793–2796, 1998a.

Kärcher, B., R. Busen, A. Petzold, F.P. Schröder, U. Schumann, and E.J. Jensen, Physico-chemistry of aircraft-generated liquid aerosols, soot, and ice particles, 2. Comparisons with observations and sensitivity studies, *J. Geophys. Res., 103*, 17,129–17,147, 1998b.

Kärcher, B., Aviation-produced aerosols and contrails, *Surv. Geophys., 20*, 113–167, 1999.

Lukachko, S.P., I.A. Waitz, R.C. Miake-Lye, R.C. Brown, and M.R. Anderson, Production of sulfate aerosol precursors in the turbine and exhaust nozzle of an aircraft engine, *J. Geophys. Res., 103*, 16159–16174, 1998.

Miake-Lye, R.C. et al., SO_x oxidation and volatile aerosol in aircraft exhaust plumes depend on fuel sulfur content, *Geophys. Res. Lett., 25*, 1677–1680, 1998.

Petzold, A., A. Döpelheuer, C.A. Brock, and F.P. Schröder, In situ observations and model calculations of black carbon emissions by aircraft at cruise altitude, *J. Geophys. Res., 104*, 22,171–22,181, 1999.

Schröder, F.P., B. Kärcher, A. Petzold, R. Baumann, R. Busen, C. Hoell, and U. Schumann, Ultrafine aerosol particles in aircraft plumes: In situ observations, *Geophys. Res. Lett., 25*, 2789–2792, 1998.

Schröder, F.P., C.A. Brock, R. Baumann, A. Petzold, R. Busen, P. Schulte, and M. Fiebig, In situ studies on volatile jet exhaust particle emission – Impacts of fuel sulfur content and thermodynamic conditions on nuclei mode aerosols, *J. Geophys. Res., 105*, in press, 2000.

Schumann, U., H. Schlager, F. Arnold, R. Baumann, P. Haschberger, and O. Klemm, Dilution of aircraft exhaust plumes at cruise altitudes, *Atmos. Environ., 32*, 3097–3103, 1998.

Seinfeld, J.H., Clouds, contrails and climate, *Nature, 391*, 837–838, 1998.

Slemr, F., H. Giehl, J. Slemr, R. Busen, P. Schulte, and P. Haschberger, In flight measurements of aircraft nonmethane hydrocarbon emission indices, *Geophys. Res. Lett., 25*, 321–324, 1998.

Tremmel, H.G., and U. Schumann, Model simulations of fuel sulfur conversion efficiencies in an aircraft engine: Dependence on reaction rate constants and initial species mixing ratios, *Aerosp. Sci. Technol., 3*, 417–430, 1999.

Turco, R.P., and F. Yu, Particle size distributions in an expanding plume undergoing coagulation and condensation, *J. Geophys. Res., 104*, 19,227–19,242, 1999.

Weisenstein, D.K., G.K. Yue, M.K.W. Ko, N.D. Sze, J.M. Rodriguez, and C.J. Scott, A two-dimensional model of sulfur species and aerosols, *J. Geophys. Res., 102*, 13,019–13,035, 1997.

Yu, F., and R.P. Turco, The role of ions in the formation and evolution of particles in aircraft plumes, *Geophys. Res. Lett., 24*, 1927–1930, 1997.

Yu, F., R.P. Turco, and B. Kärcher, The possible role of organics in the formation and evolution of ultrafine aircraft particles, *J. Geophys. Res., 104*, 4079–4087, 1999.

Bernd Kärcher and Reinhold Busen, DLR, Institut für Physik der Atmosphäre, D-82234 Wessling, Germany. (bernd.kaercher@dlr.de.)

Richard P. Turco and Fangqun Yu, UCLA, Department of Atmospheric Sciences, Los Angeles, CA 90095, USA.

Micheal Y. Danilin and Debra K. Weisenstein, Atmospheric and Environmental Research, Inc., Cambridge, MA 02139, USA.

Richard C. Miake-Lye, Aerodyne Research, Inc., Billerica, MA 01821, USA.

[1]DLR, Institut für Physik der Atmosphäre, Wessling, Germany

[2]UCLA, Department of Atmospheric Sciences, Los Angeles, USA

[3]Atmospheric and Environmental Research, Inc., Cambridge, USA

[4]Aerodyne Research, Inc., Billerica, USA

This preprint was prepared with AGU's LaTeX macros v4. File top formatted March 16, 2000.

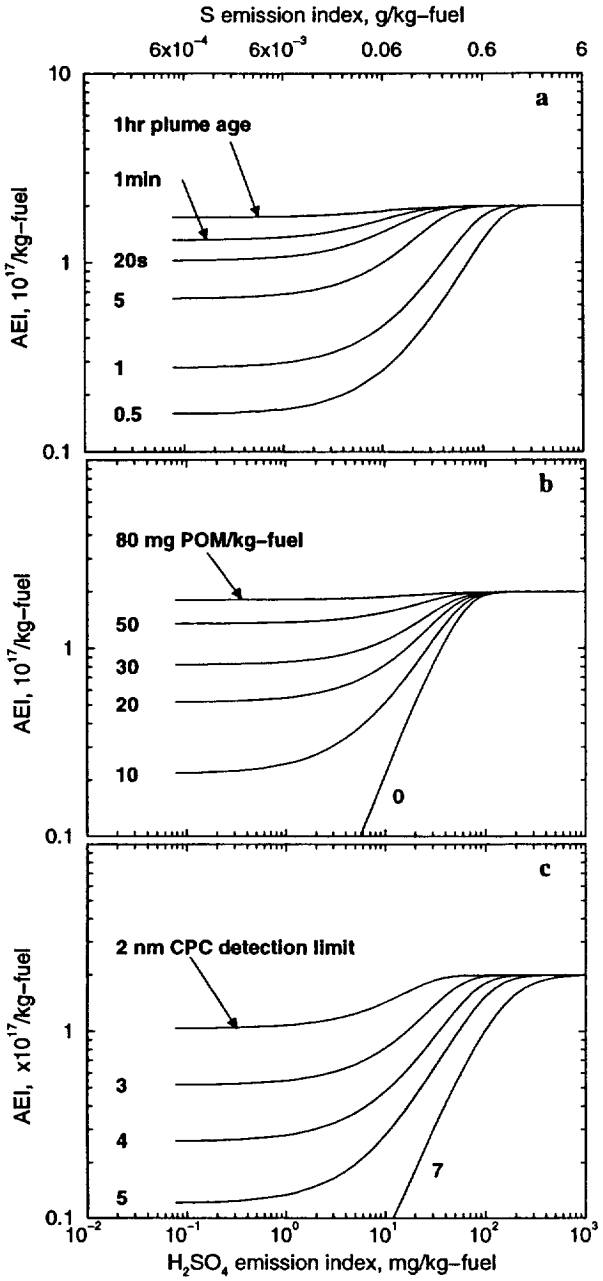

Figure 1. Apparent ultrafine volatile particle emission indices versus H_2SO_4 emission index (lower abscissa) and S emission index (upper ascissa). Default values used in the analytical model (solid curves) are: $N_i = 2 \times 10^{17}$/kg-fuel, $\eta = 0.05$, $D_{th} = 3\,\mathrm{nm}$, EI(POM) = 20 mg/kg-fuel, and $t = 3\,\mathrm{s}$. a: Plume age t is varied from 0.5 s up to 1 hr. b: Emission index of condensable organic species EI(POM) is varied from 0–80 mg/kg-fuel. c: Lower cut-off diameter D_{th} (50 % detection efficiency) of ultrafine particle counter is varied from $2 - 7\,\mathrm{nm}$.

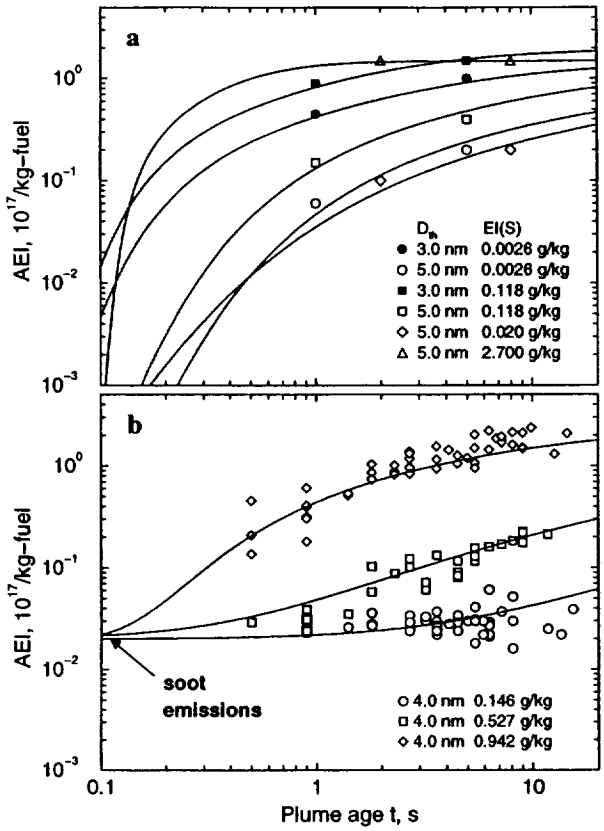

Figure 2. Observed ultrafine particle emission indices (symbols) versus plume age. The legends denote CNC detection limits and fuel S contents. The corresponding curves are results from the model described here. a: Data taken during the DLR SULFUR 5 and 6 field missions behind the ATTAS aircraft. For the calculations, we use η = 0.03–0.06 depending on EI(S) taken from a detailed chemical model [*Brown et al.*, 1996] and N_i = (1.5–2) $\times 10^{17}$/kg-fuel [*Schröder et al.*, 1998]. We used the basically unknown parameter EI(POM) within the range 20–30 mg/kg-fuel to fit the data. Only volatile AEIs are shown. b: Same as in Figure 2a, but for the F-16 aircraft. Data taken during the NASA Subsonic Assessment Near-Field Interaction Flight (SNIF III) Experiment [*Anderson et al.*, 1999]. Model curves obtained with $\eta = 0.005 - 0.01$, N_i = (3–4) $\times 10^{17}$/kg-fuel, and EI(POM) = 1 mg/kg-fuel. The SNIF data include non-volatile soot particles which show comparatively little variability. Therefore, the soot AEIs added to the volatile AEIs create a baseline value of 2×10^{15} particles per kg-fuel.

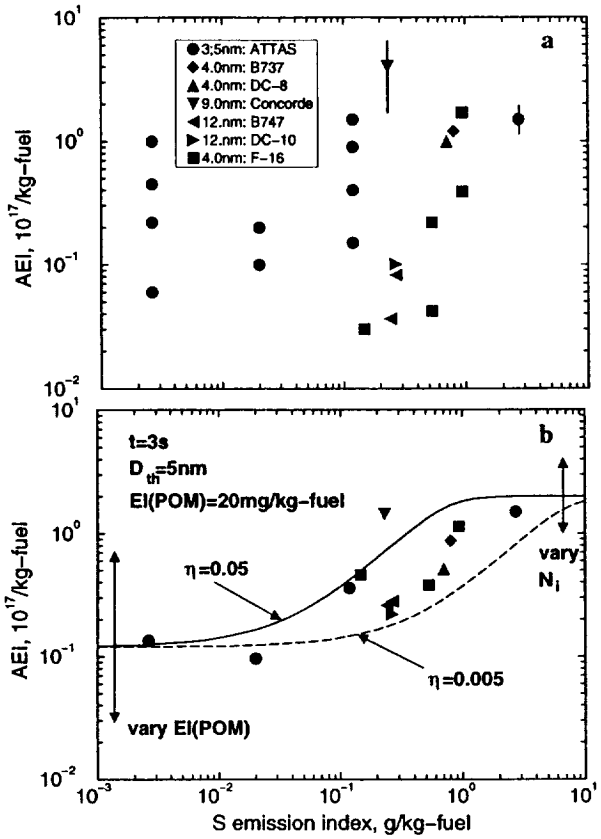

Figure 3. Emission indices of detectable volatile particles versus fuel S content. Aircraft were examined as part of several missions in Europe and the United States of America. Aircraft types and values for D_{th} are indicated in the legend. Besides the data shown in Figure 2, we include a subset of data (those where no contrails formed during the observations) corresponding to plume ages up to 2 min (Concorde: up to 1 hr) discussed by the *IPCC* [1999]. a: Data plotted irrespective of plume ages, CNC detection limits, and organic emissions. The vertical bar at the rightmost data point indicates the approximate spread of most of the subsonic data. For the Concorde (uppermost triangle and bar), this variability is much larger [*Fahey et al.*, 1995]. b: Same data as in Figure 3a, but normalized to $t = 3$ s, $D_{th} = 5$ nm, and 20 mg POM/kg-fuel, after being fitted to (1) and (2) as in Figure 2. The curves emphasizing the trend of observed AEIs with increasing EI(S) are model results at the same values for t, D_{th}, and EI(POM), with $N_i = 2 \times 10^{17}$/kg-fuel and $\eta = 0.05$ (solid curve) or $\eta = 0.005$ (dashed curve). Varying EI(POM) and N_i causes the curves to shift, as indicated by the arrows; the resulting shifts are not strictly proportional to EI(S).

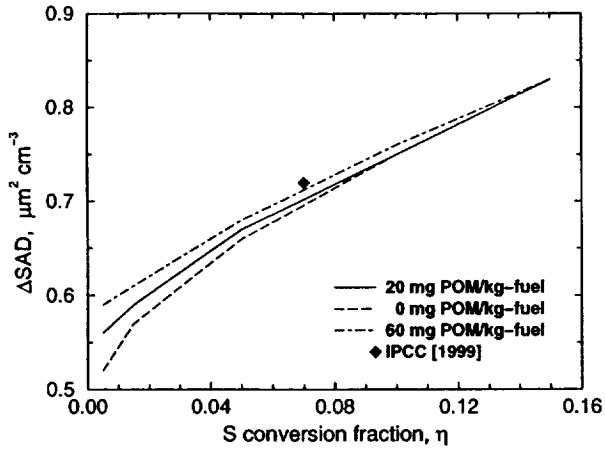

Figure 4. Calculated changes in sulfate aerosol surface area density in the region of maximum perturbation (32–90°N, 14–18.5 km altitude) versus S conversion fraction at the engine exit for a future (2015 scenario) supersonic fleet. The perturbation should be compared with the simulated background value of $0.9\,\mu m^2\,cm^{-3}$. Curves represent calculations with our novel approach, using 0, 20, and 60 mg POM/kg-fuel. The diamond represents the simplified treatment used in the *IPCC* [1999] assessment, repeated for 0.4 g S/kg-fuel and assuming $\eta = 0.1$ and monodisperse particles with $D = 20$ nm as the input for the global model, in lieu of aerosol processing on the scale of the plume. The diamond is plotted by estimating the engine exit plane value of η which would give $\eta = 0.1$ after plume processing. Gas phase chemical conversion of emitted SO_2 to H_2SO_4 and subsequent condensation adds about 0.02 per day to η.

Appendix 2

Parameterization of OH for Efficient Computation in Chemical Tracer Models

B. Duncan, D. Portman, I. Bey and C. Spivakovsky

JOURNAL OF GEOPHYSICAL RESEARCH, VOL. 105, NO. D10, PAGES 12,259–12,262, MAY 27, 2000

Parameterization of OH for efficient computation in chemical tracer models

Bryan Duncan

Department of Earth and Planetary Sciences and Division of Engineering and Applied Sciences, Harvard University, Cambridge, Massachusetts

David Portman

Atmospheric and Environmental Research (AER), Inc., Cambridge, Massachusetts

Isabelle Bey and Clarissa Spivakovsky

Department of Earth and Planetary Sciences and Division of Engineering and Applied Sciences, Harvard University, Cambridge, Massachusetts

Abstract. We present a parameterization for the tropospheric concentration of the hydroxyl radical (OH) which can be used to overcome the costs of solving kinetic equations in chemical tracer models. This parameterization accurately represents OH predicted by a full chemical mechanism. The 24-hour average concentration of OH is represented as a set of high-order polynomials in variables such as temperature, latitude, declination, and the concentrations of ozone, water vapor, carbon monoxide, nitrogen oxides (as a family), and hydrocarbons. The parameterization of OH consists of computer-written FORTRAN functions for an efficient computation of the polynomials. The parameterization of OH is publicly available.

1. Introduction

Three-dimensional (3-D) models of dynamics and chemistry have become an important tool for investigating the budgets of trace species such as ozone (O_3), nitrogen oxides (NO_t = NO + NO_2 + $2N_2O_5$ +NO_3 + HNO_2 + HNO_4), hydroxyl radical (OH), and methane (CH_4) [e.g., *World Meteorological Organization (WMO)*, 1999]. As computing power has increased, these models have become more complex, particularly in terms of the detail of the chemical schemes, and have moved toward higher vertical and spatial resolution. Many initial studies relied on short (1-2 year) simulations, but several problems of interest require longer simulations, for example, examination of the causes of trends in trace gases. Despite the increases of computing power, parameterizations of model processes designed to enhance computational efficiency are still necessary. One such parameterization, that of the chemistry of the OH radical, was developed in the late 1980s by *Spivakovsky et al.* [1990a].

When the primary sink of a species is reaction with OH, a parameterization of OH can be used to overcome the expense of solving chemical kinetic equations. *Spivakovsky et al.* [1990a] presented a method used to define a set of polynomials describing the functional dependence of tropospheric OH on chemical, radiative, and meteorological variables. *Spivakovsky et al.* [1990b] then applied this method to a 3-D simulation of methylchloroform. Using the same method, *Jacob et al.* [1993] and *Wang et al.* [1998] parameterized photolysis rates and chemical production and loss rates of various tracers such as O_3, OH, and NO_t.

Paper number 1999JD901141.
0148-0227/00/1999JD901141$09.00

The parameterization of OH by *Spivakovsky et al.* [1990a] is out of date because of significant changes recommended recently for key reactions affecting OH concentrations, including a non-negligible quantum yield for $O(^1D)$ at wavelengths between 312 to 320 nm [*Talukdar et al.*, 1998] and a decrease in the rate of reaction of OH with CH_4 [*Gierczak et al.*, 1997]. In this paper we present an updated version of the parameterization of OH produced with a current and detailed mechanism of O_3, NO_t and hydrocarbon chemistry [*Jaeglé et al.*, 1999]. We include the dependence of OH on isoprene and several other hydrocarbons omitted by Spivakovsky et al. We improved the method of Spivakovsky et al. by further automating the parameterization procedure. The parameterization of OH developed here is intended for use in studies of factors controlling distributions and temporal trends of tropospheric carbon monoxide (CO) and CH_4, but can also be applied to studies of other chemical species where reaction with OH is the primary sink.

2. Generation of the Parameterization

Spivakovsky et al. [1990a] created their polynomial functions by calculating the least squares fit (LSF) to results of a large number of point-model calculations. A 0-D photochemical model with an accurate kinetic solver was used to generate the point-model calculations. These calculations were performed across the entire multidimensional domain defined by ranges of independent variables, such as O_3, CO, water vapor, and NO_t. Computer-generated FORTRAN functions for evaluation of the polynomials were returned as result of this procedure, as well as estimates of the accuracy achieved for an independent set of points. If the accuracy was found to be insufficient, the domain space was divided manually (i.e., off-line) into rectangular subdomains, and the parameterization procedure was repeated. (The domain space

is divided because at a certain stage in the selection process, augmentation of additional terms no longer improves the accuracy significantly.) Divisions of the domain into subdomains were chosen based on the knowledge at that time of the dependence of OH on various independent variables, such as water vapor, O_3, and NO_t. The choice of divisions within a subdomain was often an educated trial-and-error process because it is nearly impossible for a human mind to conceptualize the dependence of a function on a large number of independent variables.

In an effort to make the parameterization procedure less labor-intensive and more efficient, we implemented a computerized search for optimal divisions within a subdomain, proposed (but not implemented) by *Spivakovsky et al.* [1990a]. This automated procedure is more efficient because it searches for divisions across the domain space (i.e., multidimensional divisions). While divisions with respect to only one independent variable will remove some of the nonlinearity in a system, the best divisions for OH chemistry usually lie across the subdomain space and involve correlations of independent variables [*Sillman et al.*, 1990]. As a result, fewer divisions are required to achieve a desired accuracy. The division procedure is outlined below.

The N-dimensional domain is divided into two parts by a plane

$$\sum_{i=1}^{N} a_i x_i + a_{N+1} = 0 \qquad (1)$$

where x_i denote parameters. Coefficients a_i (for $i = 1, \ldots, N+1$) are obtained as a solution to the following optimization problem. Define function $\rho(a_1, \ldots, a_{N+1})$ as a root-mean-square error (RMS) for a piece-polynomial function composed of two second-order polynomials with a separate LSF polynomial for each of the two parts of the domain:

Table 1. Independent Variable Ranges Used in the Parameterization of OH

Independent Variables	Ranges
Pressure, mbar[a]	800-1020, 350-800, 100-350
Temperature, K	depends on season, altitude, latitude
Chemical Variables	
NO_t, pptv[a]	1-300, 300-1000, >1000
O_3, ppbv	3-110
CO, ppbv	10-400
CH_4, ppbv[b]	600-2200
H_2O, ppmv	depends on season, altitude, latitude
Isoprene, pptv[a]	0-5000
Acetone, propane, ethane, propene, >C_4 alkanes, pptv	depends on season, altitude, latitude
Solar Irradiance Variables	
Surface Albedo (unitless)	0.05-0.8
Declination Angle, deg[a]	-23--8, -8-22, 8-23, 21-8
Latitude, deg[a,c]	0-30, 30-40, 40-60, 60-90 North and South
Cloud Albedo (unitless)[d]	0-0.6
Overhead O_3 Column, DU	200-400

DU, Dobson units.

[a]Manual divisions in range (i.e., done prior to parameterization).

[b]The range for CH_4 is expanded beyond what is expected in the current atmosphere because the present parameterization of OH is intended for use in simulations of its past, present, and future tropospheric distributions.

[c]Divisions based on resolution of O_3 climatologies of *Logan* [1999a,b].

[d]Cloud albedo has above and below components.

Table 2. RMS Errors Associated with Parameterizations Describing Surface OH under Harvard-GEOS Model Conditions for July 1994

Region	[OH], x10^5 molecules/cm^3	RMS Error, %
Tropics (30°S-30°N)		
Ocean	~10-20	<8
Land (desert)	~20-40	<8
Land (forest)	<10	8-15
Land (biomass burning)	~10-20	8-15
Midlatitudes (30°-60°N)		
Ocean	~10-20	8-10
Land	<10	8-15
Midlatitudes (30°-60°S)		
Ocean	<10	10-30
Land	<10	10-30
High latitudes (>60°N)	<10	10-20
High latitudes (>60°S)[a]	<<10	--

[a][OH] set to a climatological mean value [*Spivakovsky et al.*, 1999].

$$\sum_{i=1}^{N} a_i x_i + a_{N+1} \geq 0 \qquad (2)$$

and

$$\sum_{i=1}^{N} a_i x_i + a_{N+1} < 0 \qquad (3)$$

Determine coefficients a_i (for $i = 1, \ldots, N+1$) that define a minimum of $\rho(a_1, \ldots, a_{N+1})$. We used the simplex method of multidimensional minimization [*Nelder and Mead*, 1965; *Press et al.*, 1989] to solve for a_i. Multiple calls to the LSF procedure are necessary for solving this minimization problem; however, for a second-order polynomial these calls are inexpensive. (To facilitate this process, the LSF procedure is interfaced with the point-model calculation to generate additional points as needed.) After the plane of optimal subdivision is determined, the full procedure with selection of appropriate higher-order terms is carried out for each subdivision. Construction of polynomials and division of the domain are repeated for each subdomain until the accuracy specified by the user is achieved, or until the subdomain size is less than a user-specified minimum.

3. Description of Parameterization for OH

The independent chemical, radiative, and meteorological variables chosen to describe parameterized OH are listed in Table 1. The choice of independent variables and ranges was guided by the current understanding of OH chemistry [e.g., *Logan et al.*, 1981; *Sillman et al.*, 1990; *Eisele et al.*, 1997; *Singh et al.*, 1995].

Separate parameterizations were obtained for the lower, middle, and upper troposphere (1020-800, 800-300, and 300-150 mbar) to account for differences in the chemical regime due to differences in the concentration of water, sunlight, and temperature. Parameterizations were also obtained for different seasons and latitude bands because seasonal variations can result in vastly different levels of OH and specific functional dependencies [*Kleinman*, 1991]. Due to the varying dependence of OH on the concentration of NO_t, we constructed separate parameterizations for clean, moderately polluted, and polluted regions [*Lin et al.*, 1988]. Finally, since variations in isoprene concentrations can act to reduce OH concentrations by orders of magnitude [*Jacob and Wofsy*, 1988],

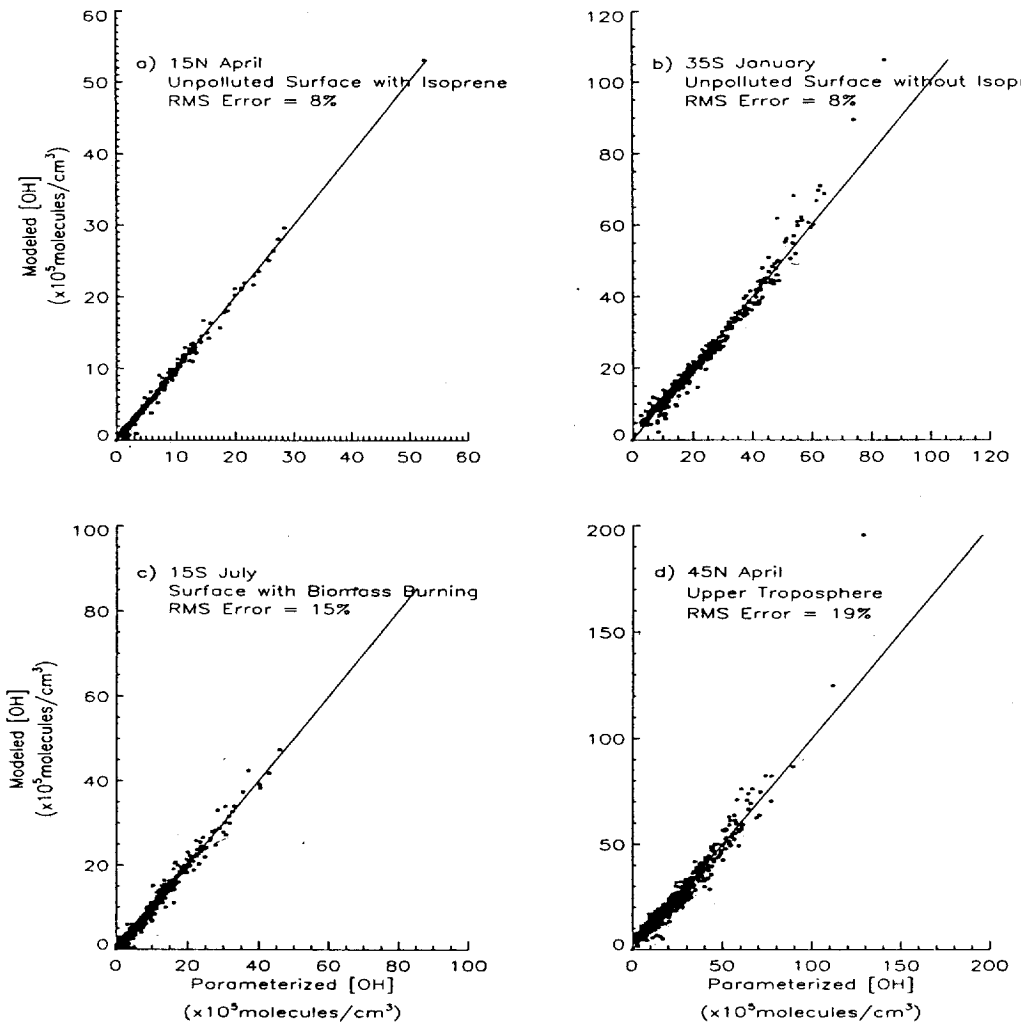

Figure 1. Parameterized OH (x10^5 molecules/cm^3) versus "true" OH from point-model calculations for four locations: (a) clean tropical surface, (b) southern midlatitude surface, (c) tropical surface affected by biomass burning, and (d) northern midlatitude upper troposphere.

we developed parameterizations with and without isoprene. Additional domain divisions were determined by the convenience of using the resolution of the O_3 and temperature climatologies of *Logan* [1999a,b] and *Randel* [1992], respectively. In total there are about 220 separate parameterizations to describe the tropospheric OH field.

Ranges for independent variables used in the parameterization are listed in Table 1. Due to a large number of individual subdomains, it is not feasible to list ranges of independent variables for each subdomain. These ranges for chemical species and physical parameters were estimated from observations and monthly average values predicted by a global model. The global model used for estimating ranges was the Harvard-GEOS model of transport and chemistry driven by assimilated meteorological data from the Goddard Earth Observing System Data Assimilation Office (GEOS-DAO) [*Bey et al.*, 1999]. Since a potential application of the parameterization of OH developed here is a study of long-term trends of tropospheric CH_4, we expanded its range to include preindustrial and possible future concentrations.

4. Results

RMS errors associated with the parameterizations used to describe the surface OH field under Harvard-GEOS model conditions for a day in July 1994 are shown in Table 2. The RMS error given in percent of the mean OH for the sample is used as a measure of accuracy. Since removal by OH of CO, CH_4, and other long-lived species occurs predominantly in the tropics [*Logan et al.*, 1981], the highest accuracy was required for 30°S to 30°N. We also required higher accuracy in midlatitudes during summer because of high concentrations of OH in this season. We tolerated lower accuracies where OH concentrations are generally suppressed due, for instance, to high isoprene emissions. In these regions of low OH we chose not to invoke further divisions by the parameterization procedure (i.e., to decrease the RMS for the subdomain). In subdomains where OH is very low or negligible due to low sunlight (e.g., high latitudes in winter), concentrations of OH were set to climatological mean values as a function of latitude, altitude, and season [*Spivakovsky et al.*, 1999]. Lower accu-

racies (15-45%) were also tolerated for parameterizations of the upper troposphere (not shown in Table 2) because rates of reaction of OH with CO and CH_4 (i.e., two trace gases intended for study using the parameterization of OH) are relatively small compared to lower tropospheric rates.

Figure 1 shows parameterized OH versus "true" OH from point-model calculations for four subdomains. Since the least squares method minimizes the sum of squares of deviations from the "true" points, the polynomial fit within a subdomain for higher values of OH results in smaller relative errors than for lower values.

5. Summary

Building on the method of *Spivakovsky et al.* [1990a], we have constructed an up-to-date parameterization of OH which accurately represents concentrations of OH predicted by a full mechanism of O_3, NO_t, and hydrocarbon chemistry. This new parameterization incorporates current chemical kinetic and photochemical data, and accounts for reactions of hydrocarbons with OH. The computational cost of simulating tropospheric OH is reduced by about a factor of 500 when the full chemical mechanism is replaced by the parameterization of OH. The parameterization of OH is publicly available from our website (http://www-as.harvard.edu/chemistry/trop/index.html).

Acknowledgments. We are grateful to Bob Yantosca for his patience and guidance on the computer programming aspect of our work. We thank Andrew Fusco and Jennifer Logan for important discussions during development of the parameterization for OH. This work was funded with support from the National Air and Space Administration, grant NASA-NAG1-1909 and NAG5-3665, and the National Science Foundation, grant ATM-9320778.

References

Bey, I., R. Yantosca, and D. Jacob, Export of pollutants from eastern Asia: A simulation of the PEM-West B aircraft mission using a 3-D model driven by assimilated meteorological fields (abstract), *Eos Trans. AGU, 80*(17), Spring Meet. Suppl., 31, 1999.

Eisele, F., G. Mount, D. Tanner, A. Jefferson, R. Shetter, J. Harder, and E. Williams, Understanding the production and interconversion of the hydroxyl radical during the tropospheric OH photochemistry experiment, *J. Geophys. Res., 102*, 6457-6465, 1997.

Gierczak, T., R. Talukdar, S. Herndon, G. Vaghjiani, and A. Ravishankara, Rate coefficients for the reactions of hydroxyl radical with methane and deuterated methanes, *J. Phys. Chem., 101*(17), 3125-3134, 1997.

Jacob, D., and S. Wofsy, Photochemistry of biogenic emissions over the Amazon forest, *J. Geophys. Res., 93*, 1477-1486, 1988.

Jacob, D., et al., Simulation of summertime ozone over North America, *J. Geophys. Res., 98*, 14,797-14,816, 1993.

Jaeglé, L., et al., Photochemistry of HO_x in the upper troposphere at northern midlatitudes, *J. Geophys. Res., 105*, 3877-3892, 2000.

Kleinman, L., Seasonal dependence of boundary layer peroxide concentrations: The low and high NO_x regimes, *J. Geophys. Res., 96*, 20,721-20,733, 1991.

Kleinman, L., Low and high NO_x tropospheric photochemistry, *J. Geophys. Res., 99*, 16,831-16,838, 1994.

Lin, X., M. Trainer, and S. Liu, On the nonlinearity of the tropospheric ozone production, *J. Geophys. Res., 93*, 15,879-15,888, 1988.

Logan, J., M. Prather, S. Wofsy, and M. McElroy, Tropospheric chemistry: A global perspective, *J. Geophys. Res., 86*, 7210-7254, 1981.

Logan, J., An analysis of ozonesonde data for the troposphere: Recommendations for testing 3-D models and development of a gridded climatology for tropospheric ozone, *J. Geophys. Res., 104*, 16,115-16,149, 1999a.

Logan, J., An analysis of ozonesonde data for the lower stratosphere: Recommendations for testing models, *J. Geophys. Res., 104*, 16,151-16,170, 1999b.

Nelder, J., and R. Mead, A simplex method for function minimization, *Comput. J., 7*, 308, 1965.

Press, W., B. Flannery, S. Teukolsky, and W. Vetterling, *Numerical Recipes: The Art of Scientific Computing*, pp. 289-293, Cambridge Univ. Press, New York, 1989.

Randel, W., Global atmospheric circulation statistics, 1000-1 mb, 256 pp., *NCAR Tech. Note 366, Natl. Cent. for Atmos. Res., Boulder, Colo.*, 1992.

Sillman, S., J. Logan, and S. Wofsy, The sensitivity of ozone to nitrogen oxides and hydrocarbons in regional ozone episodes, *J. Geophys. Res., 95*, 1837-1851, 1990.

Singh, H., M. Kanakidou, P. Crutzen, and D. Jacob, High concentrations and photochemical fate of oxygenated hydrocarbons in the global troposphere, *Nature, 378*, 50-54, 1995.

Spivakovsky, C., S. Wofsy, and M. Prather, A numerical method for the parameterization of atmospheric chemistry: Computation of tropospheric OH, *J. Geophys. Res., 95*, 18,433-18,439, 1990a.

Spivakovsky, C., R. Yevich, J. Logan, S. Wofsy, and M. McElroy, Tropospheric OH in a three-dimensional chemical tracer model: An assessment based on observations of CH_3CCl_3, *J. Geophys. Res., 95*, 18,441-18,471, 1990b.

Spivakovsky, C., et al., Three-dimensional climatological distribution of tropospheric OH: Update and evaluation, *J. Geophys. Res.*, in press, 1999.

Talukdar, R., C. Longfellow, M. Gilles, and A. Ravishankara, Quantum yields of $O(^1D)$ in the photolysis of ozone between 289 and 329 nm as a function of temperature, *Geophys. Res. Lett., 25*, 143-146, 1998.

Wang, Y., D. Jacob, and J. Logan, Global simulation of tropospheric O_3-NO_x-hydrocarbon chemistry, 1. Model formulation, *J. Geophys. Res., 103*, 10,713-10,725, 1998.

World Meteorological Organization (WMO), Scientific assessment of ozone depletion: 1998, *Rep. 44*, Global Ozone Res. Monit. Proj., Geneva, 1999.

I. Bey, B. Duncan, and C. Spivakovsky, Department of Earth and Planetary Sciences and Division of Engineering and Applied Sciences, Harvard University, Cambridge, Massachusetts, 02138. (email: bey@io.harvard.edu; bnd@io.harvard.edu; cms@io.harvard.edu.)

D. Portman, Atmospheric and Environmental Research (AER), Inc., 840 Memorial Dr., Cambridge, Massachusetts, 02139. (email: David_Portman@aer.com.)

(Received July 23, 1999; revised November 12, 1999; accepted November 22, 1999.)

Appendix 3

Model Estimates of ER-2 Wake Composition under Cold Conditions during SOLVE

M.Y. Danilin

IPCC Report, Aviation and the Global Atmosphere, Cambridge Univ. Press, 1999.

Schumann, U., et al., Dilution of aircraft exhaust plumes at cruise altitudes, *Atm. Env.*, *32*, 3097-3103, 1998.

Yu, F., and R.P. Turco, The formation and evolution of aerosols in stratospheric aircraft plumes: Numerical simulations and comparison with observations, *J. Geophys. Res.*, *103*, 25,915-25,934, 1998.

Appendix 1. T=195K

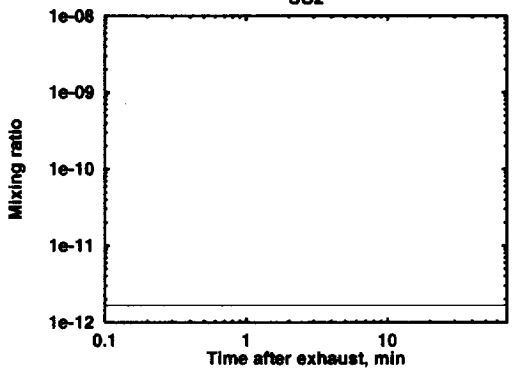

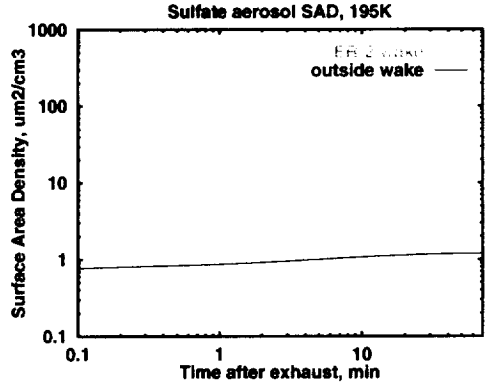

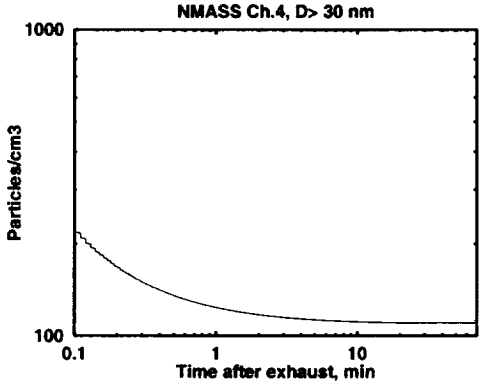

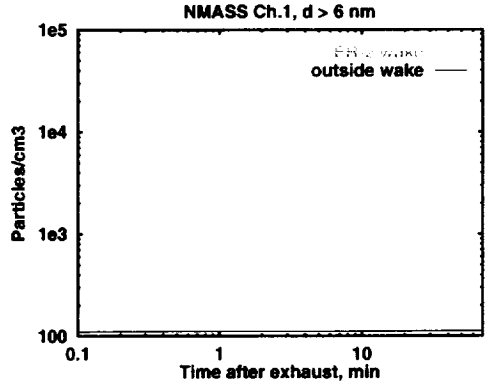

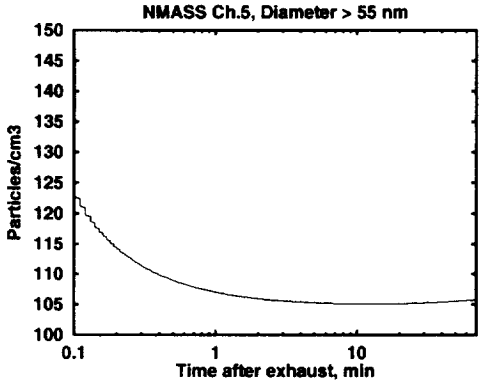

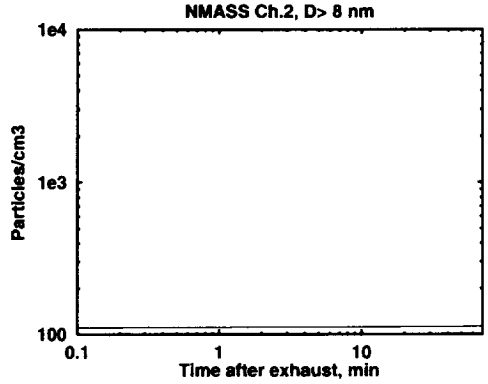

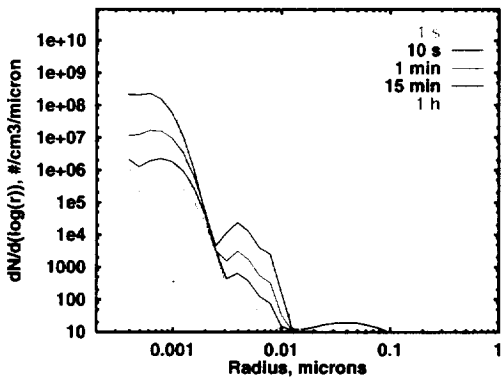

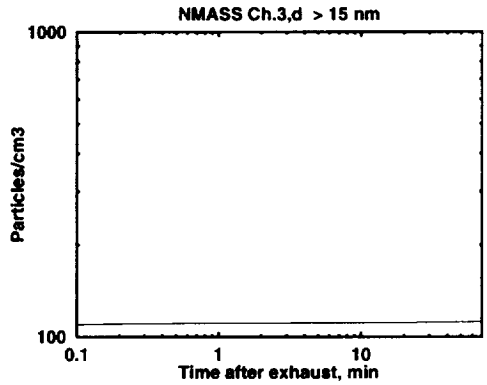

Appendix 1. T=195K

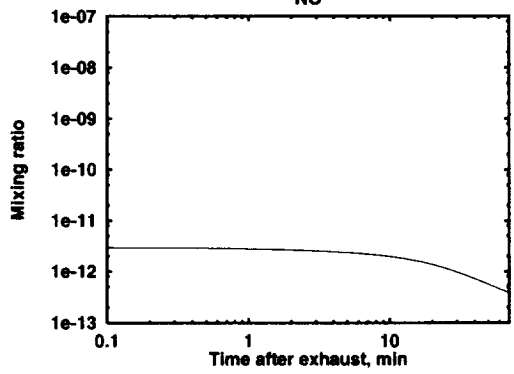

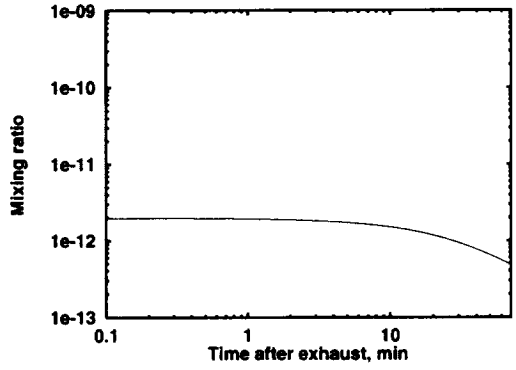

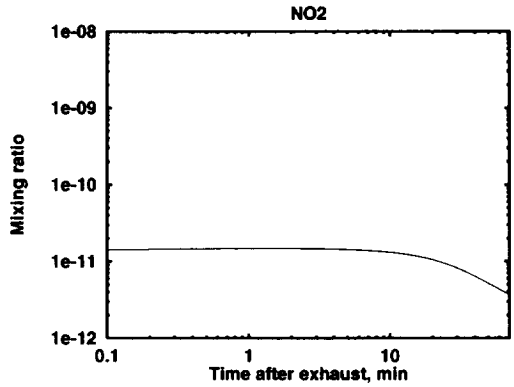

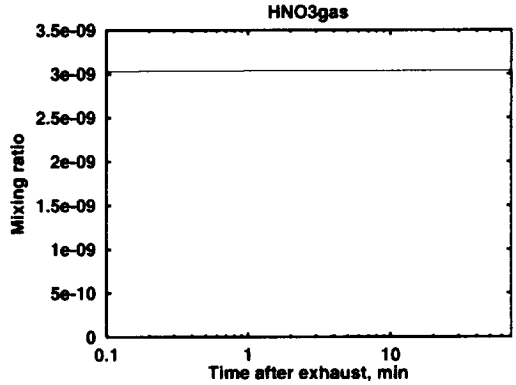

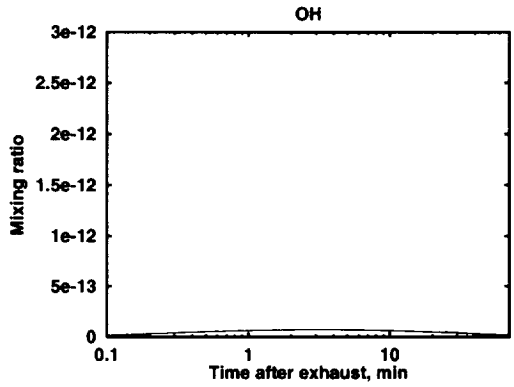

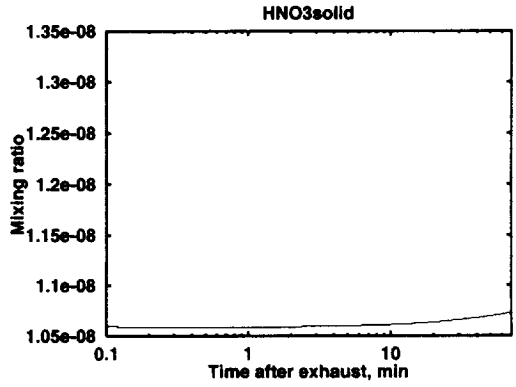

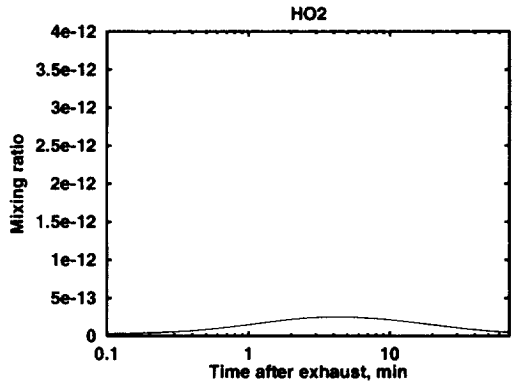

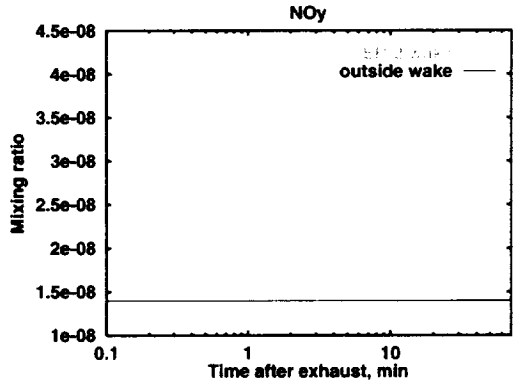

Appendix 1. T=195K

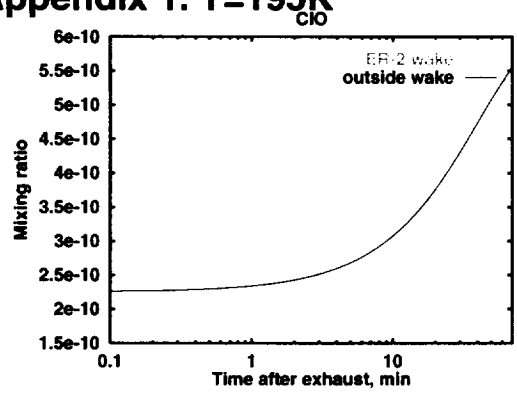

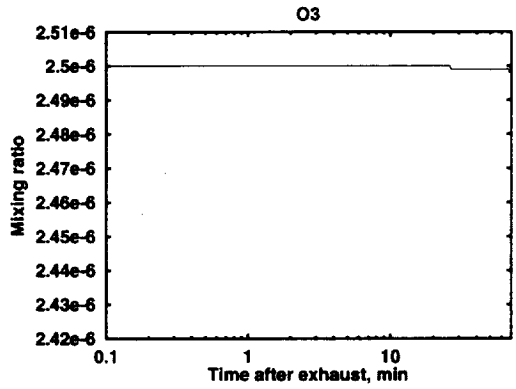

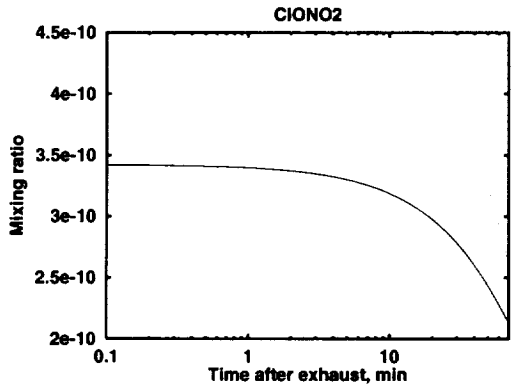

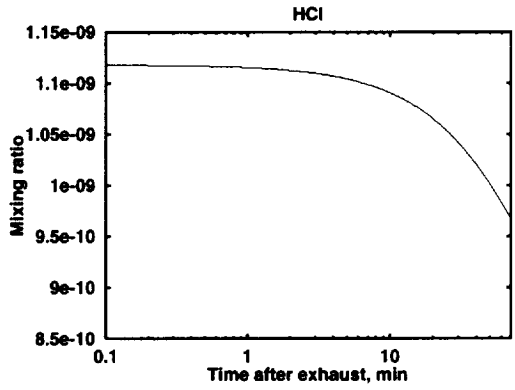

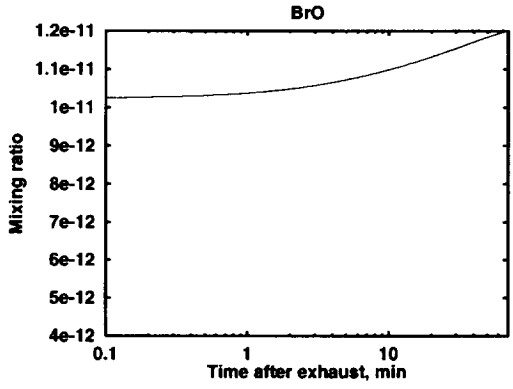

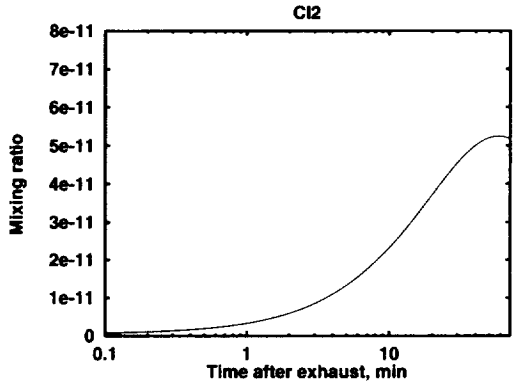

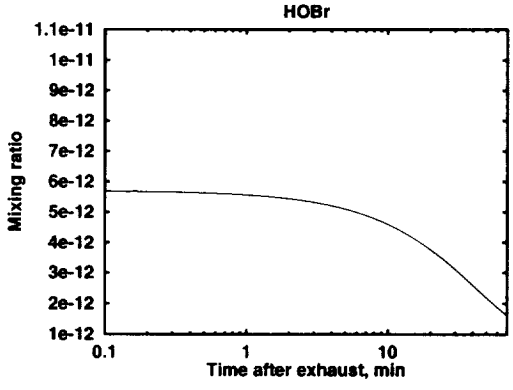

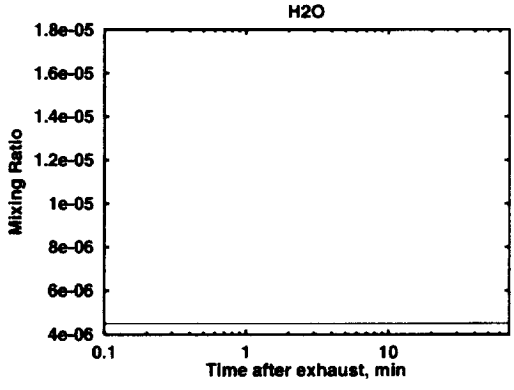

Appendix 1. T=195K

ClO

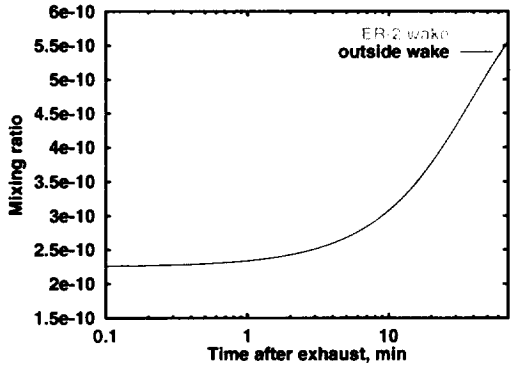

ClONO2

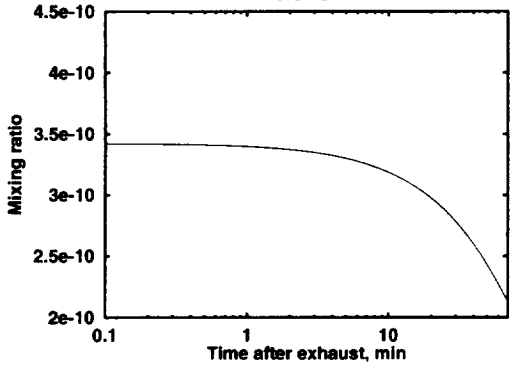

HCl

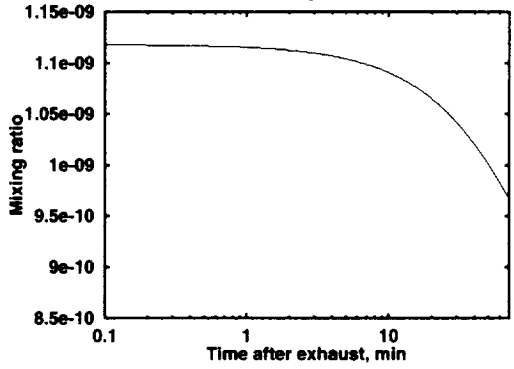

BrO

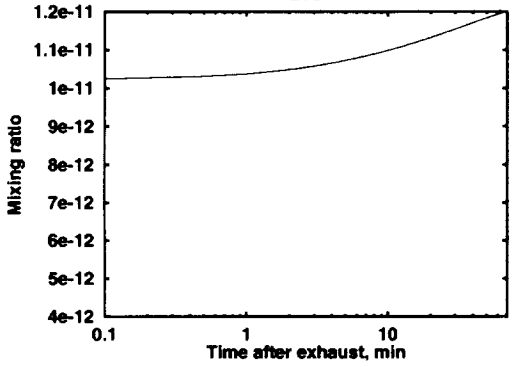

Cl2

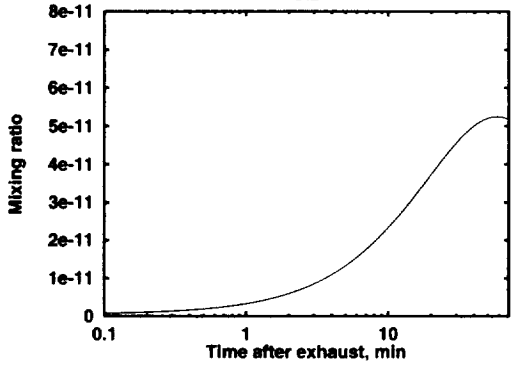

HOBr

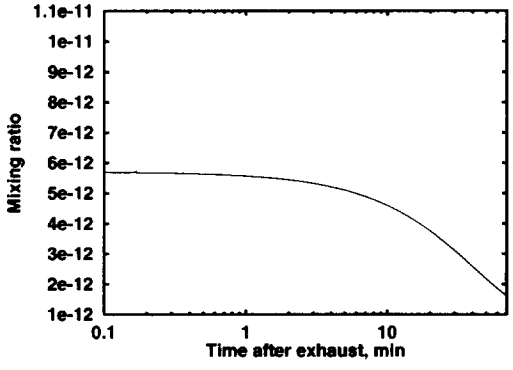

H2O

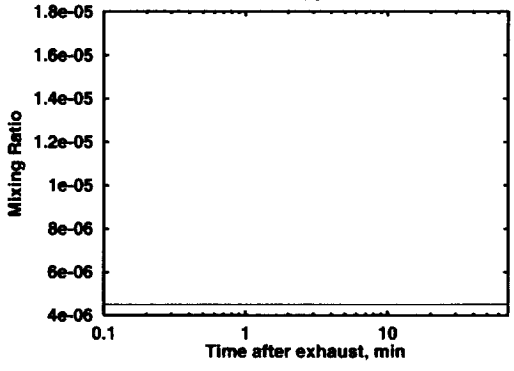

Appendix 2. T=205K

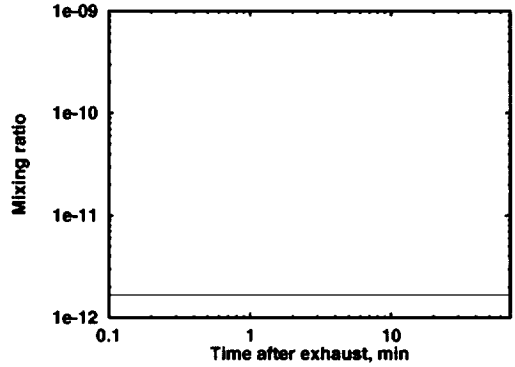

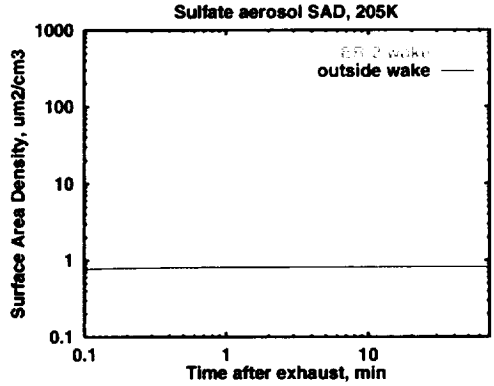

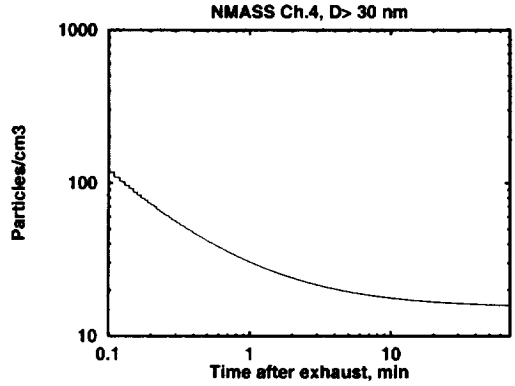

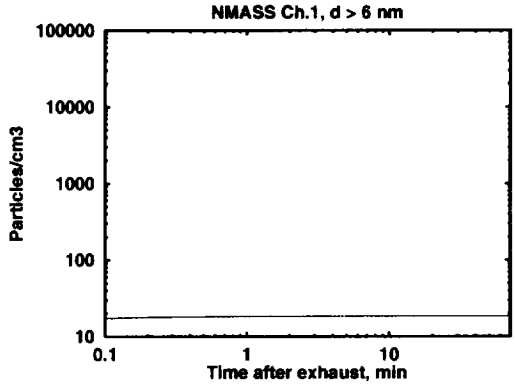

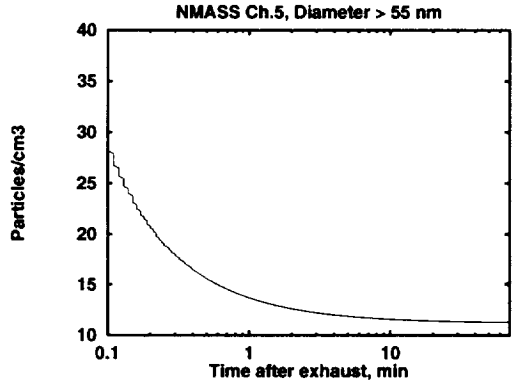

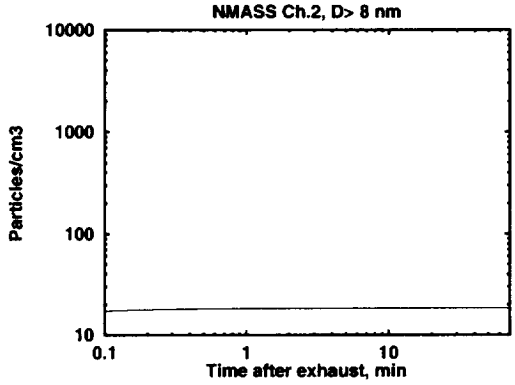

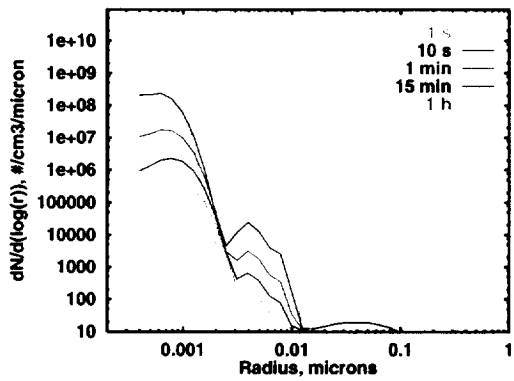

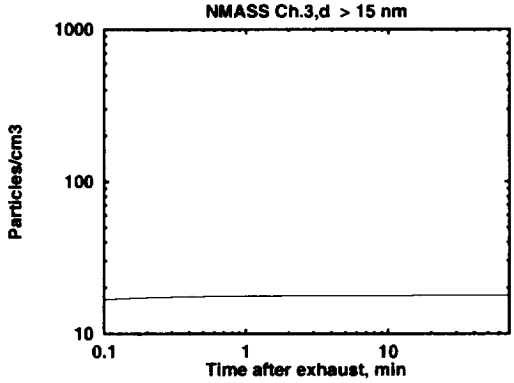

Appendix 2. T=205K

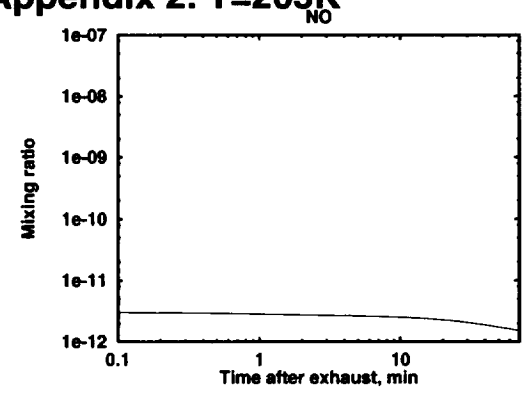

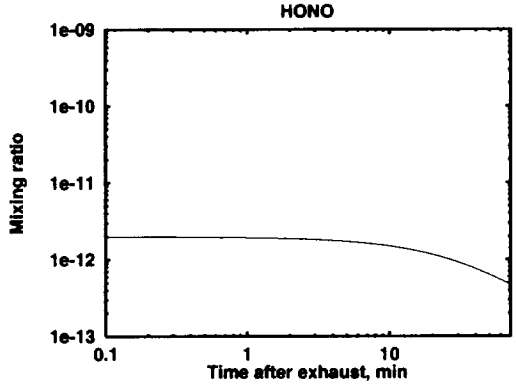

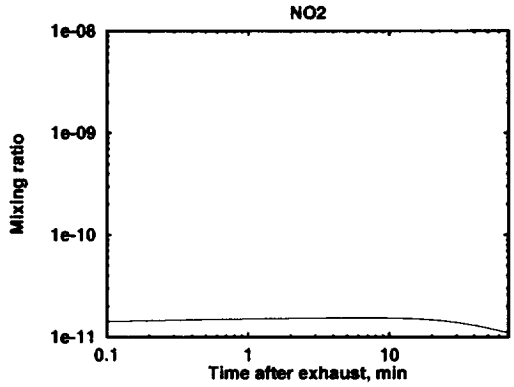

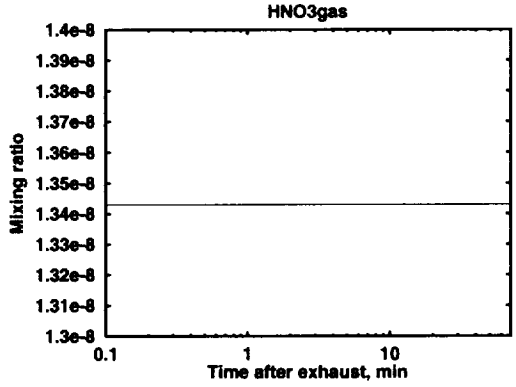

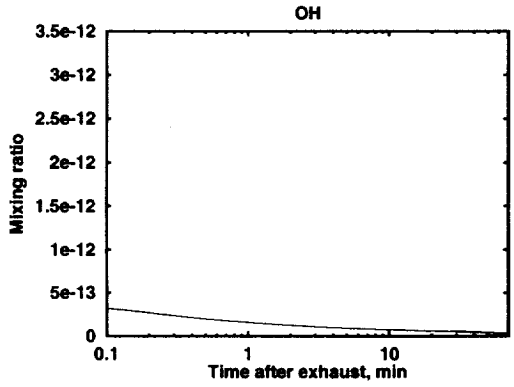

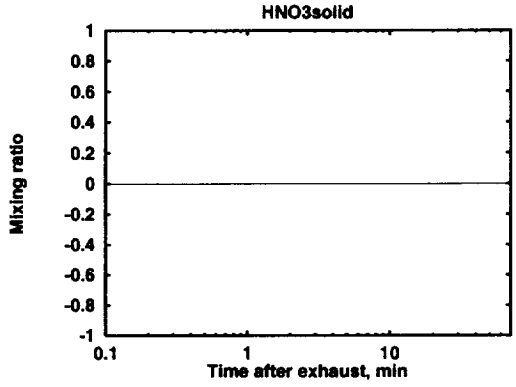

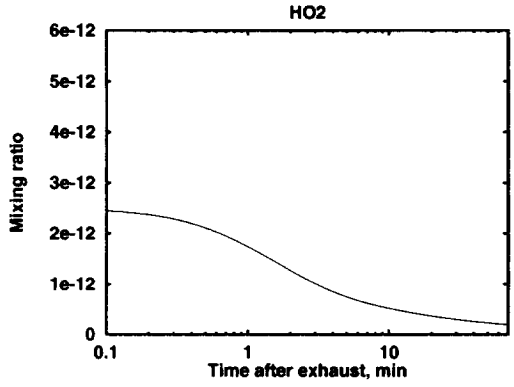

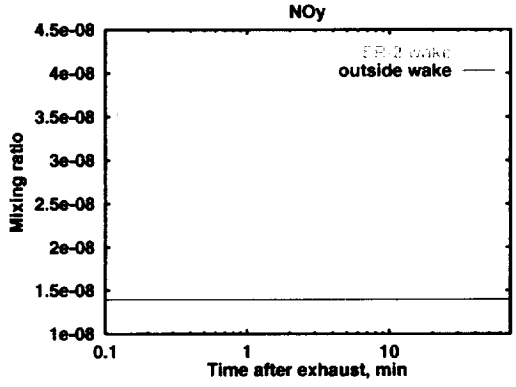

Appendix 2. T=205K

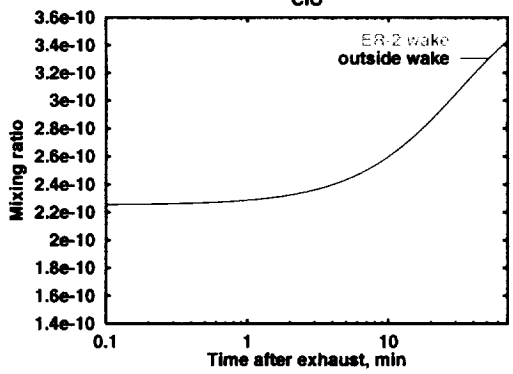

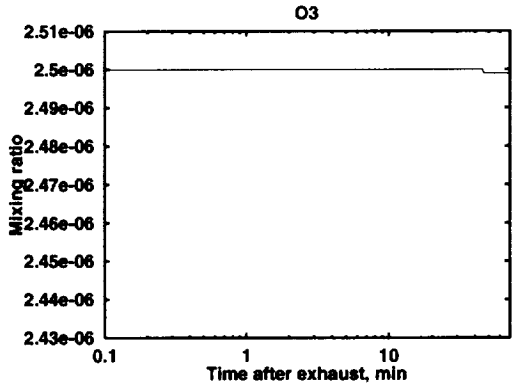

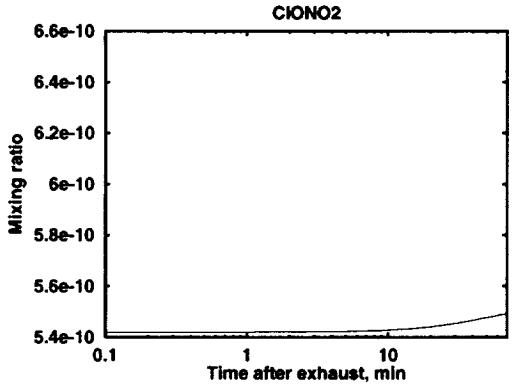

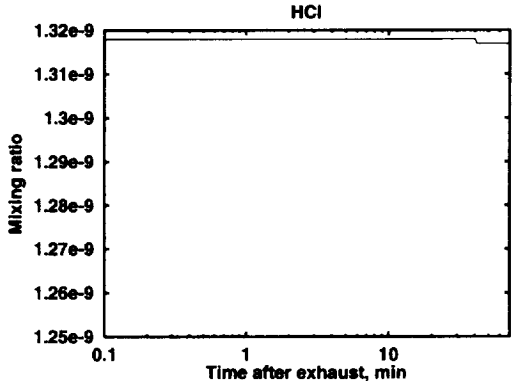

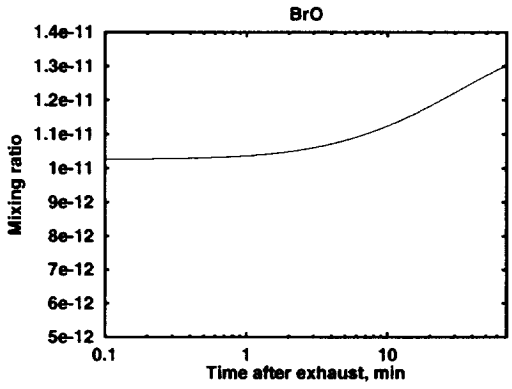

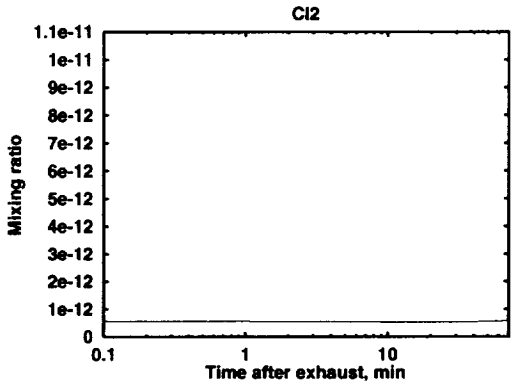

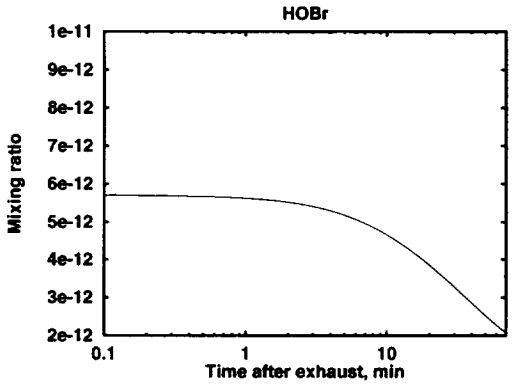

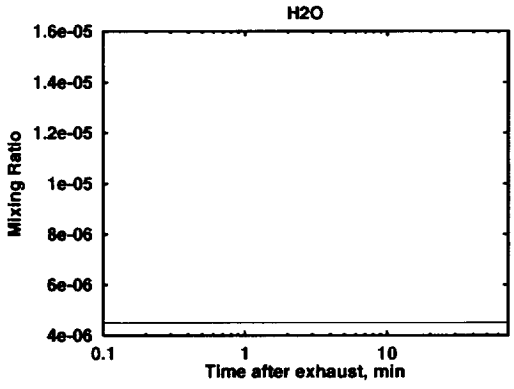

Appendix 2. T=205K

ClO

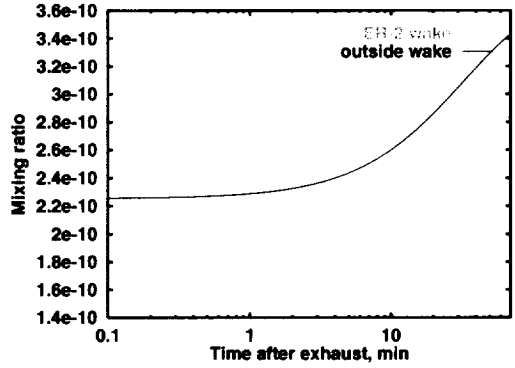

ClONO2

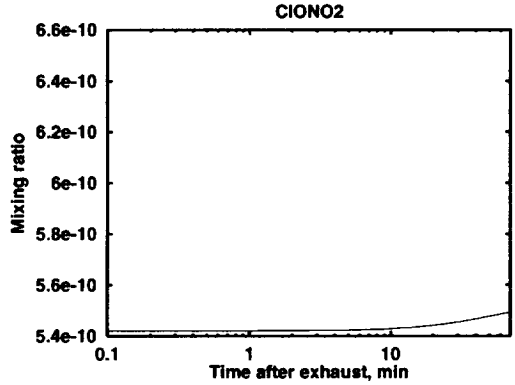

HCl

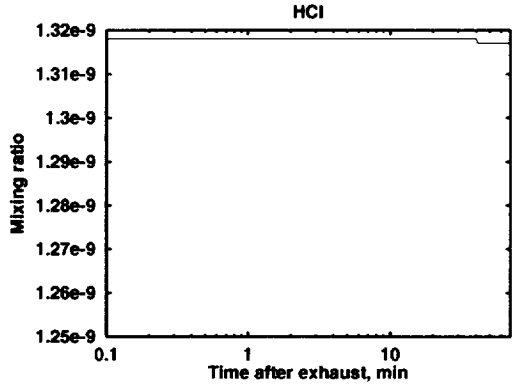

BrO

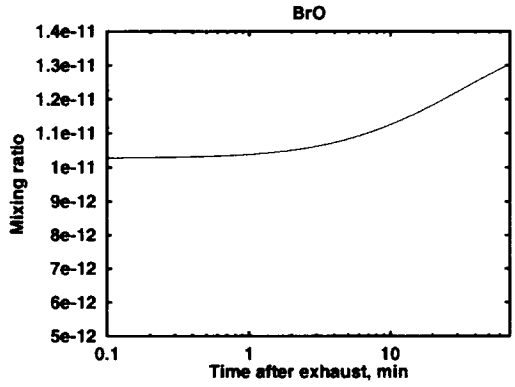

Cl2

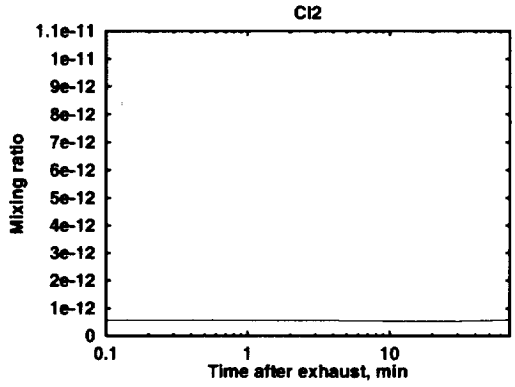

HOBr

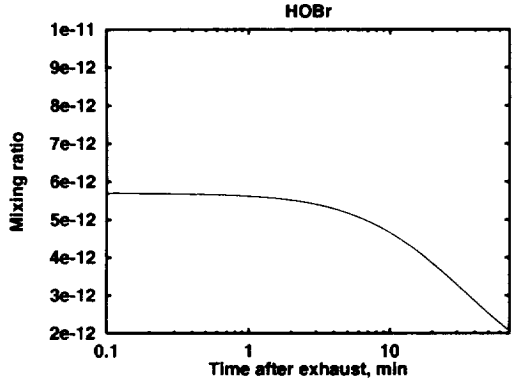

H2O

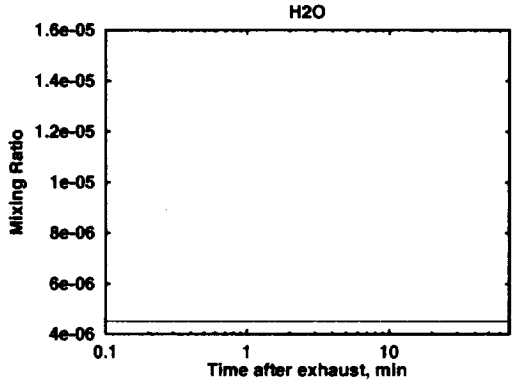

Appendix 3. T=195K

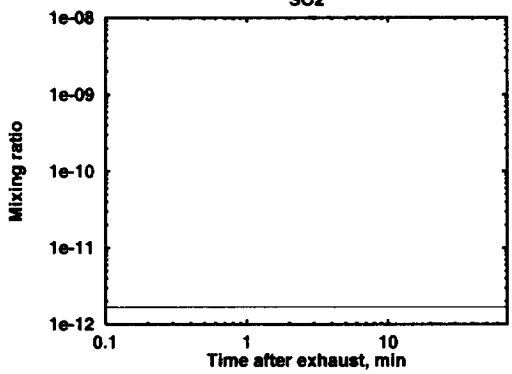

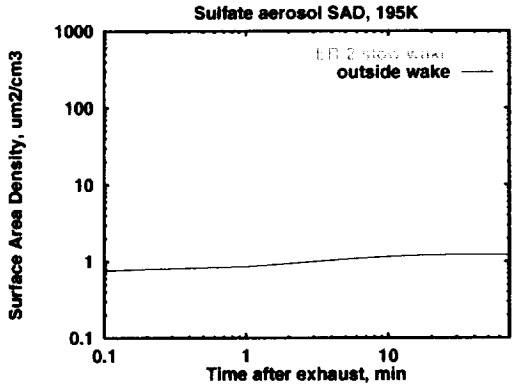

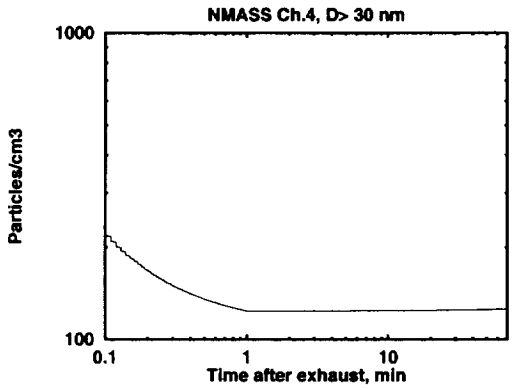

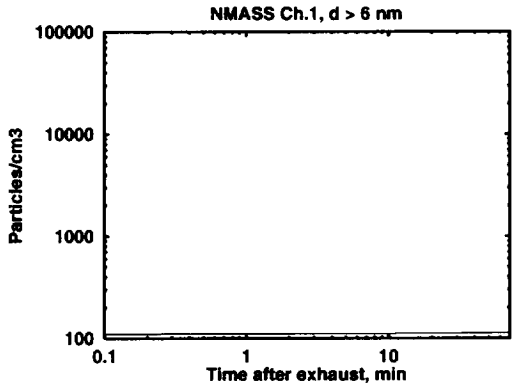

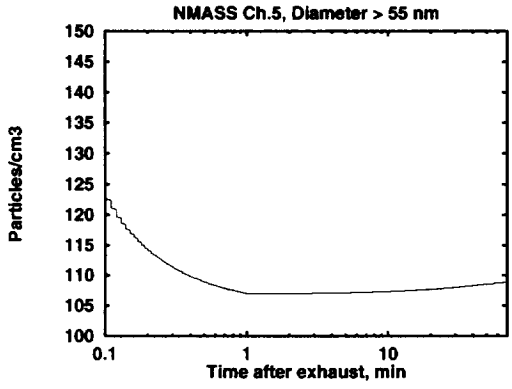

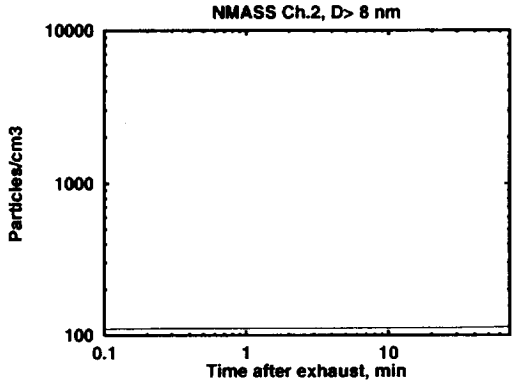

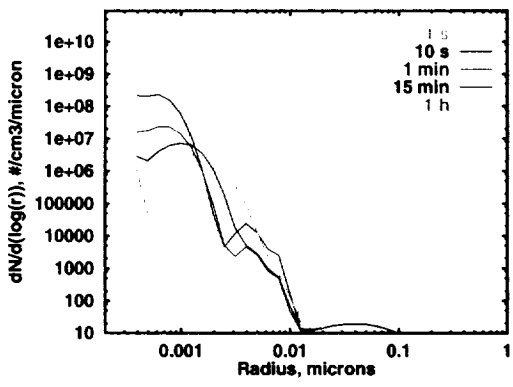

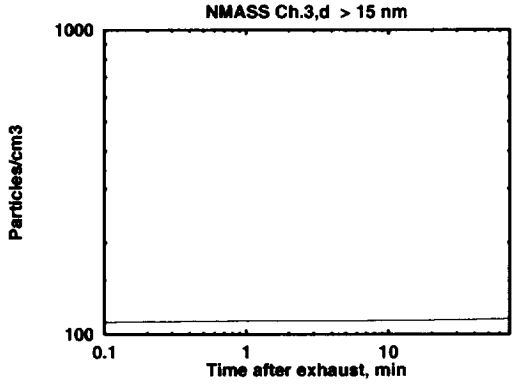

Appendix 3. T=195K

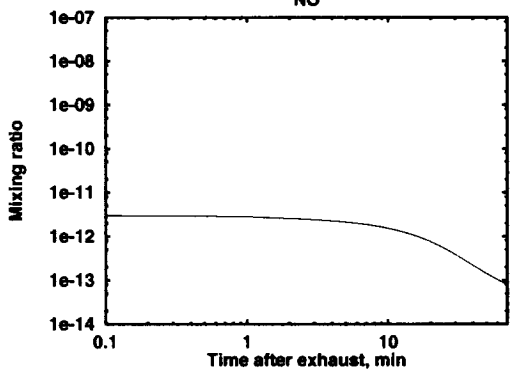

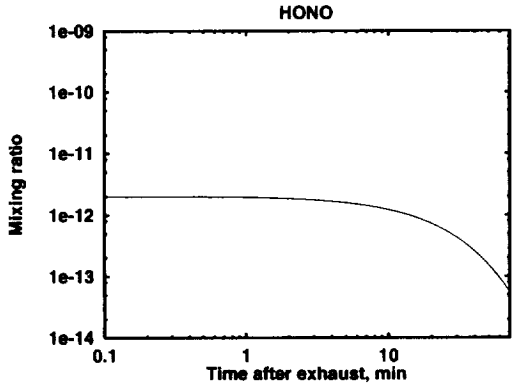

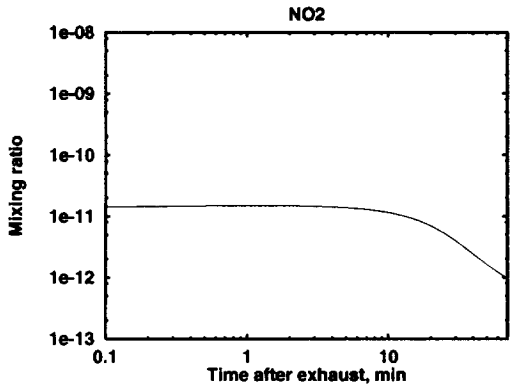

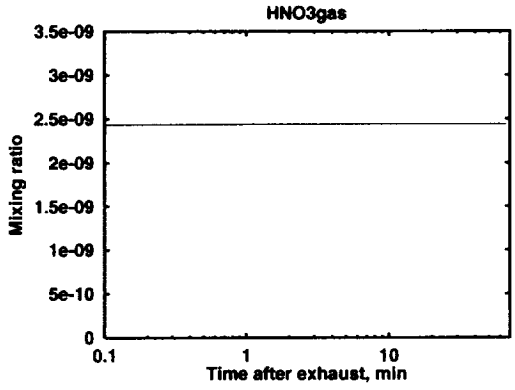

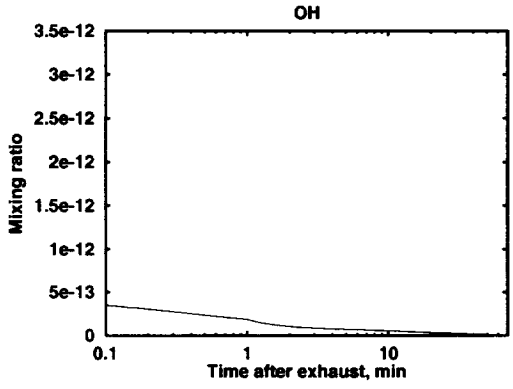

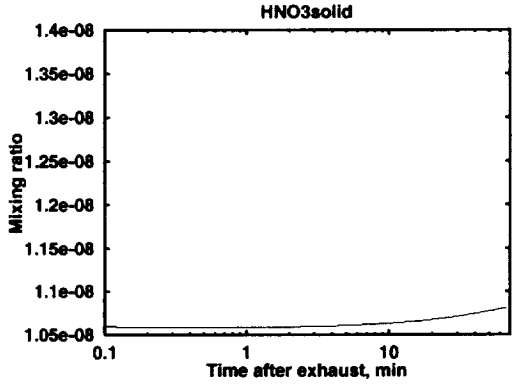

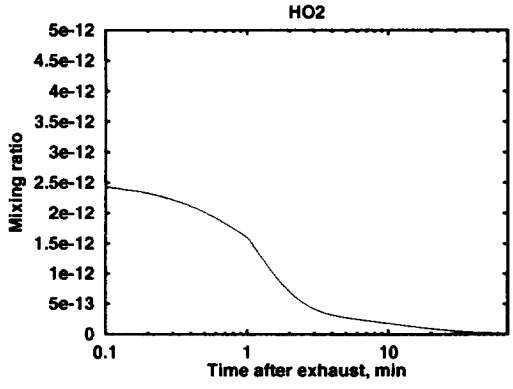

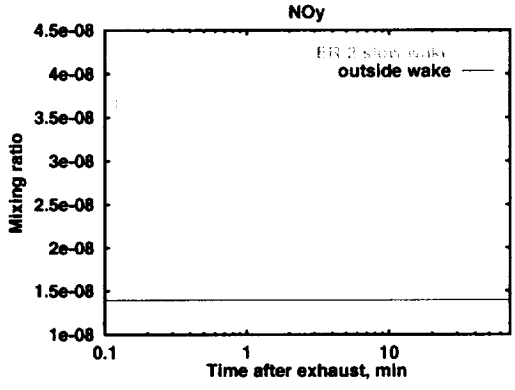

Appendix 3. T=195K

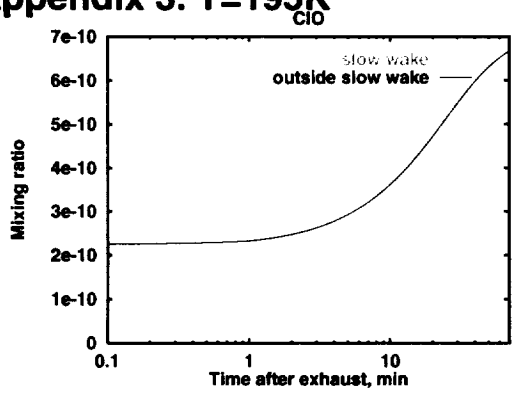

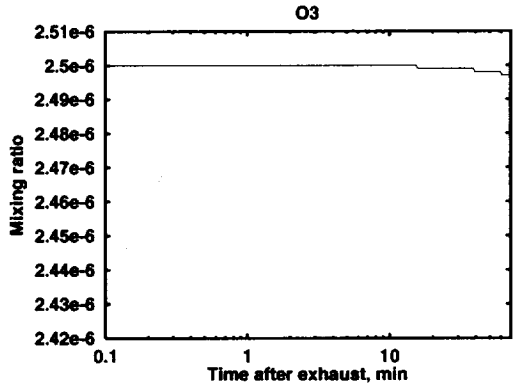

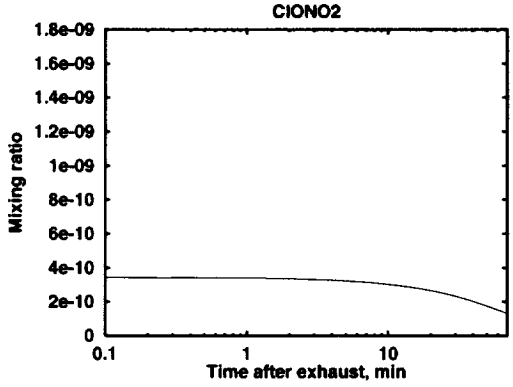

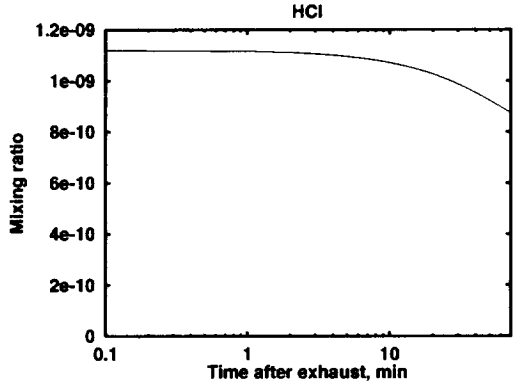

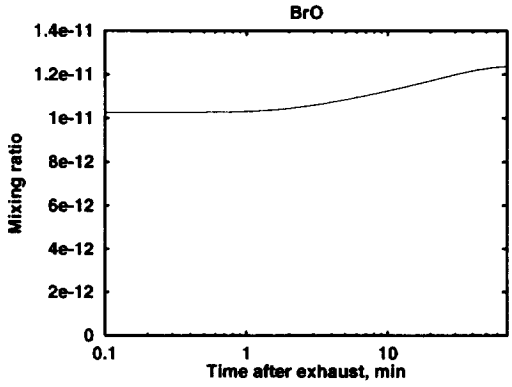

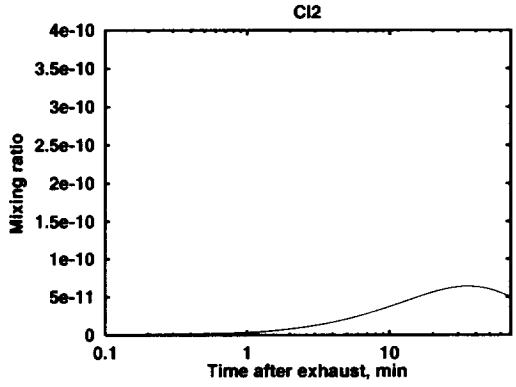

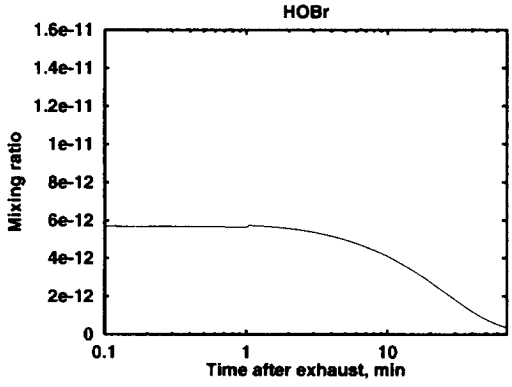

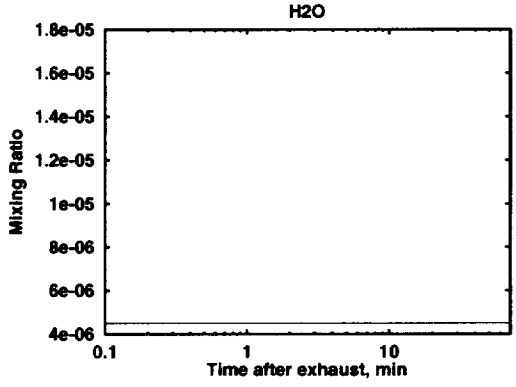

Appendix 3. T=195K

ClO

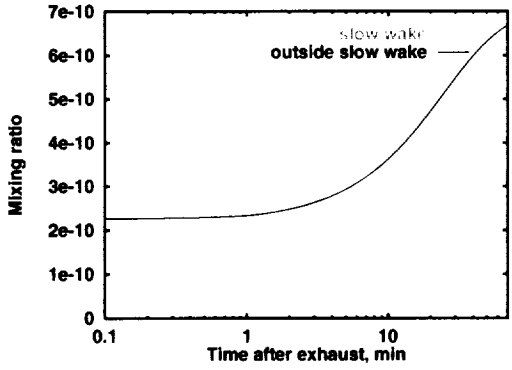

ClONO2

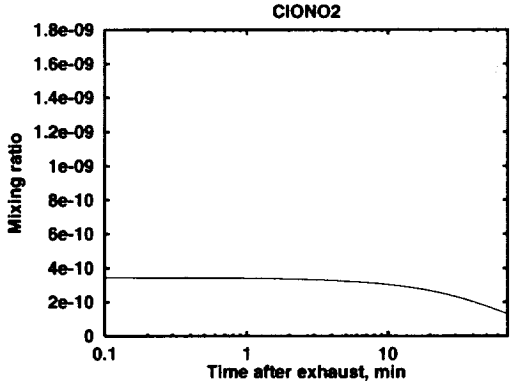

HCl

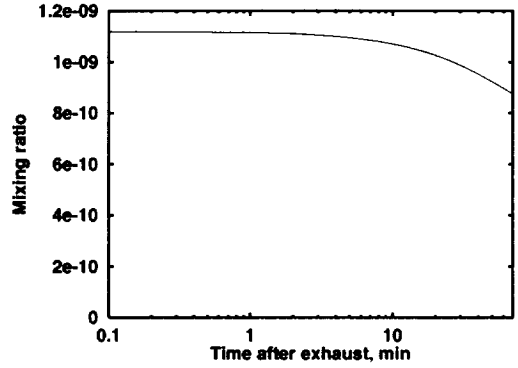

BrO

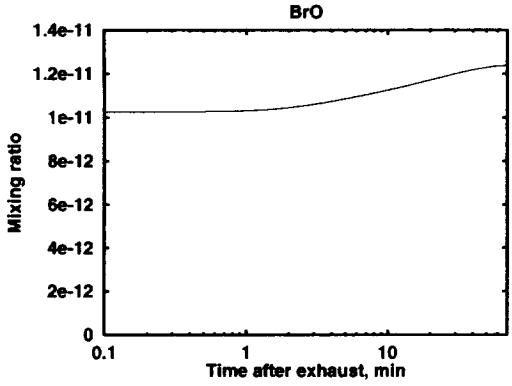

Cl2

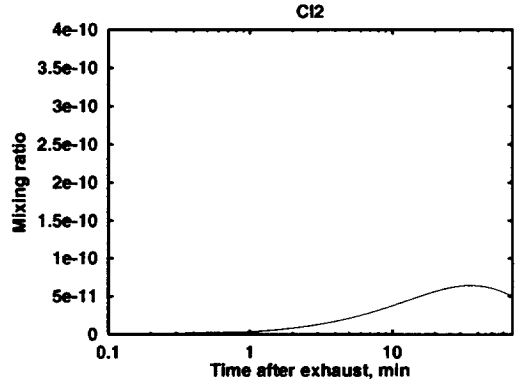

HOBr

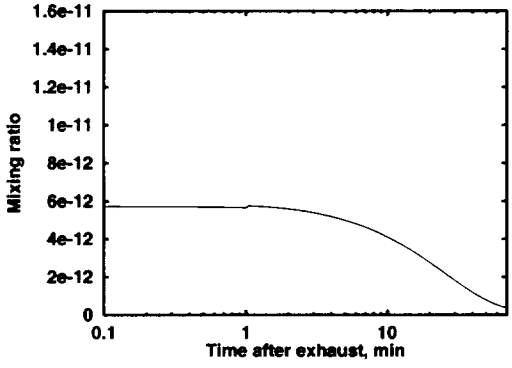

H2O

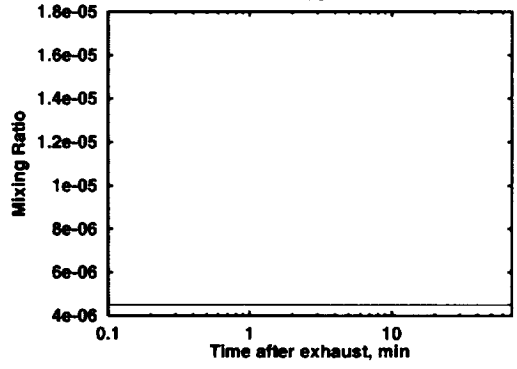

Appendix 4

Presentation at the GMI Meeting

January 2000

MKO

Possible Future Roles for 2-D models in GMI

Malcolm Ko and Charles Jackman
With inputs from AER, GSFC,a nd LLNL 2-D modeling groups

Presented at GMI ScienceTeam meeting
January 4-6 2000

Possible roles

- Participate in scientific studies such as M&M, as planning tools, as diagnostic tools
- Serve as platforms for testing components: winds, numerical scheme, chemistry, PSC, sulfate
- Sensitivity of assessment results to different transport and chemistry treatments, end to end
- 2-D transport parameters from 3-D winds. If equivalence is established, 2-D model can be used to explore parameter space.

Comparison of Model Transport

	AER	GSFC	LLNL
Grid Resolution	9.5° x 1.2 km	10° x 2.0 km	5° x 1.5 km
Transport Scheme	Smolarkiewicz	Lin and Rood	Smolarkiewicz
Advection	loosely based on obs stronger	based on 17 yr clim. weaker	clim. T, model O3 similar to AER
Horiz Diffusion - Kyy	based on correlations	consistent with adv.	consistent with adv.
Vertical Diffusion - Kzz			
troposphere	$1x10^5$ cm^2/sec	$5x10^5$-$1x10^3$ cm^2/sec	$4x10^4$ cm^2/sec
lower strat	$1x10^3$ cm^2/sec	70-$5x10^3$ cm^2/sec	2-$6x10^3$ cm^2/sec
upper strat	$1x10^4$ cm^2/sec	$5x10^3$-$1x10^5$ cm^2/sec	$6x10^3$-$1x10^5$ cm^2/sec
Kyz Diffusion	yes	no	no
Subtropical Barrier	yes	yes	yes
Polar Vortex	none	yes	yes
Age of Air	lower than obs.	close to obs.	lower than obs.
Differences due to		60% Advection 30% Kzz	differences small

NOY (ppbv)
M&M A-3
EI(NO_x)=10

LLNL Model

Differences about
1-3% everywhere

Transport Schemes:
LNL-Smolarkiewicz
AER-Smolarkiewicz

AER/LLNL
Model

AER Model

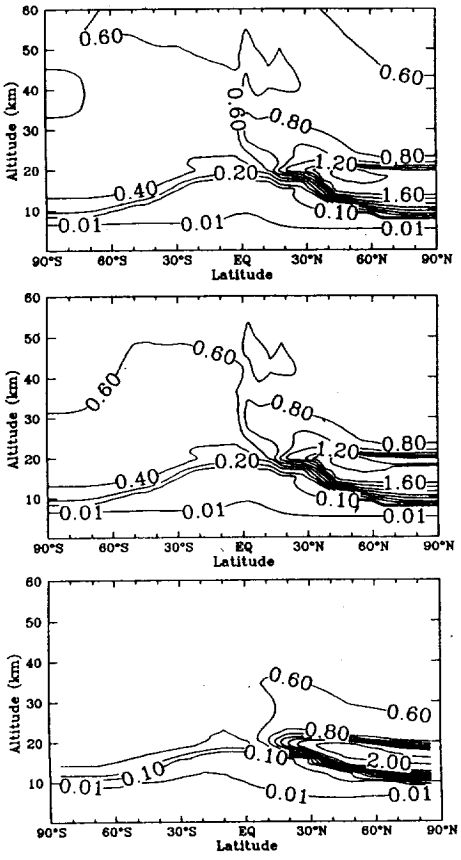

NOY (ppbv)
M&M A-3
EI(NO_x)=10

GSFC Model

Differences about
4-6% above 20 km
greater ~20 km

Transport Schemes:
GSFC-Lin & Rood
AER-Smolarkiewicz

AER/GSFC
Model

Differences due to:
Advection 50%
K_{zz} 50%

AER Model

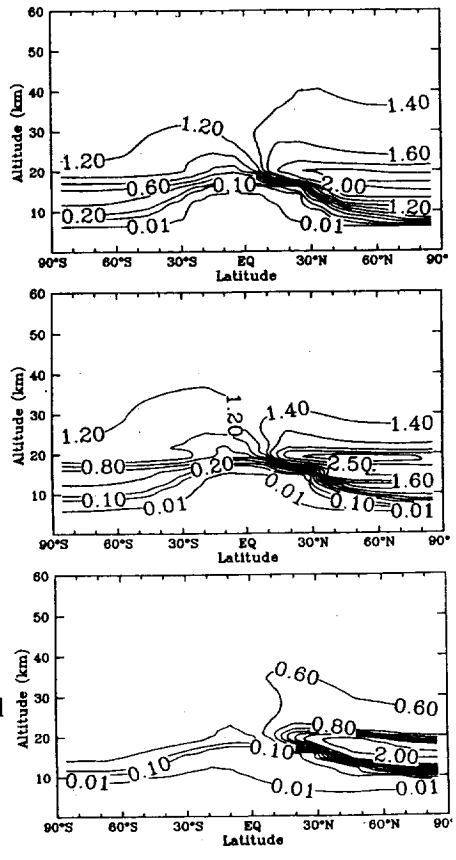

Comparison of Model Chemistry

	AER	GSFC	LLNL
Transported species	NOY, HNO3, ClY, BrY sHNO3, sH2O	NOY, HNO3, N2O5 ClONO2, ClY, BrY sHNO3, sH2O	all, non-family
Diurnal treatment	diurnal time marching for all radical species	time marching for night species only, day-avg for other species	explicit time marching
PSC Treatment	NAT, ice equilibrium	NAT, ice equilibrium	STS, climatology
Temperature Distribution	γvA	PSC SAD only	γvA
NAT Supersaturation	none	10.0	
ICE Supersaturation	none	1.4	
NAT Radius	0.5 μm	1.0 μm	
ICE Radius	7 μm	10 μm	
PSC Reactions	fixed γ	γ=fn(Rel. Hum.)	
Denitrification	localized	hemispheric	hemispheric

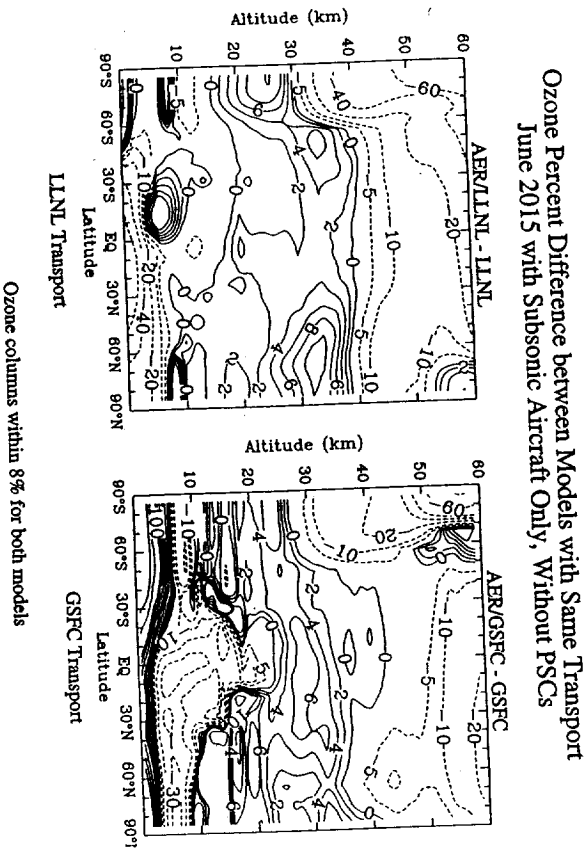

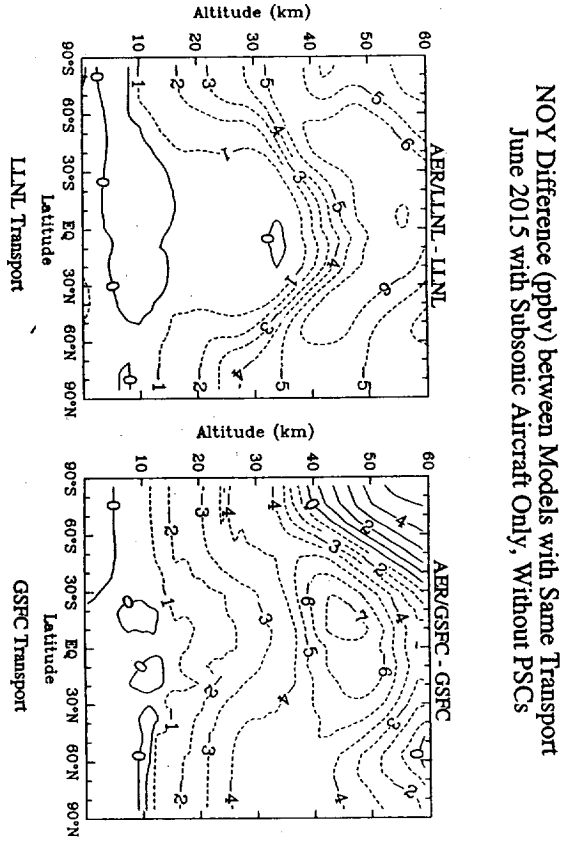

ASSESSMENT RESULTS

, Column due to HSCTs in 2015 (NO_X)=5, SA0 No PSCs

LLNL Model

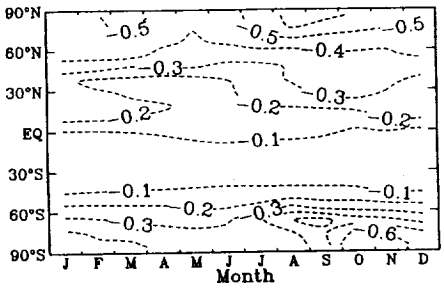

Chemical differences large in Southern Hemisphere

AER/LLNL Model

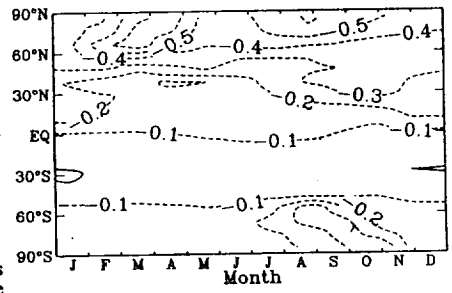

Transport differences Northern Hemisphere

AER Model

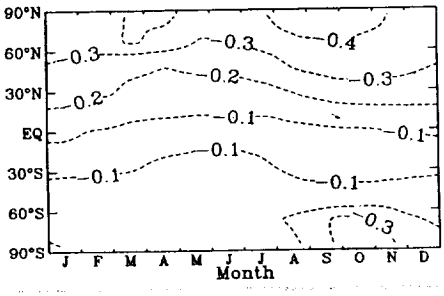

ΔO_3 Column due to 500 HSCTs in 2015 $EI(NO_X)$=5, SA0 No PSCs

GSFC Model

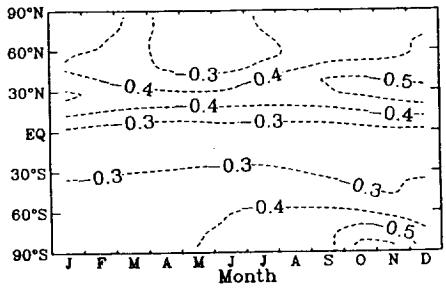

Chemical differences relatively small without PSCs

AER/GSFC Model

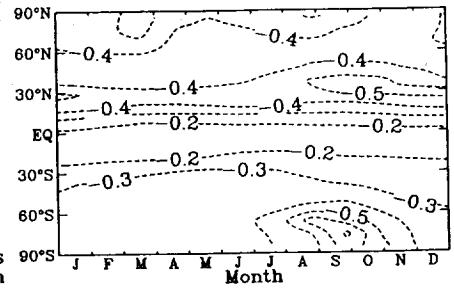

Transport differences large in Southern Hemisphere

AER Model

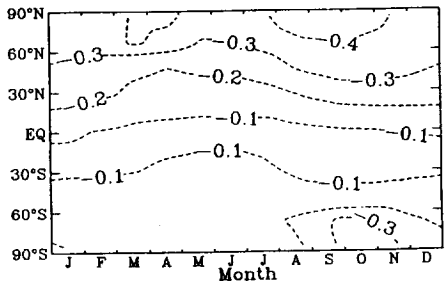

O_3 Column due to HSCTs in 2015 $I(NO_X)$=5, SA0 With PSCs

LLNL Model

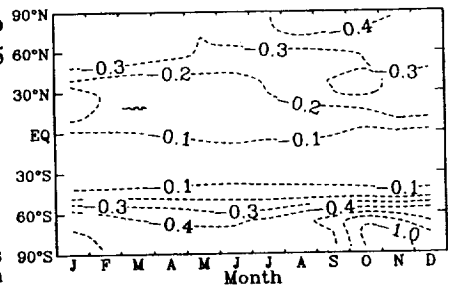

Chemical differences large in Northern Hemisphere

AER/LLNL Model

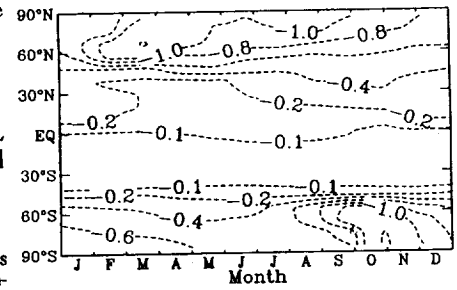

Transport differences in Northern and Southern Hemispheres

AER Model

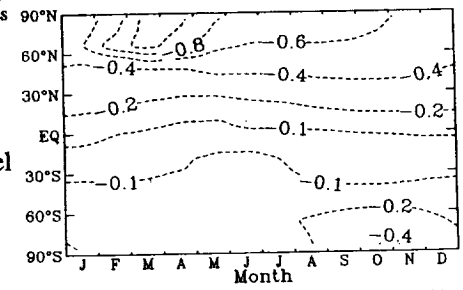

ΔO_3 Column due to 500 HSCTs in 2015 $EI(NO_X)$=5, SA0 With PSCs

GSFC Model

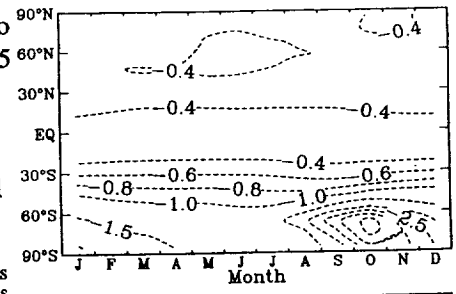

Chemical differences large with PSCs

AER/GSFC Model

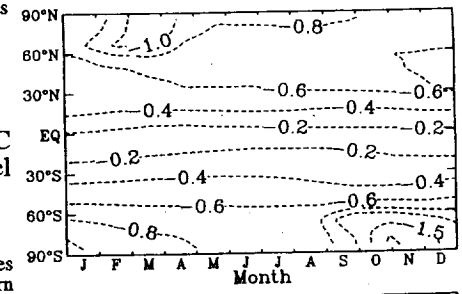

Transport differences large in Southern Hemisphere

AER Model

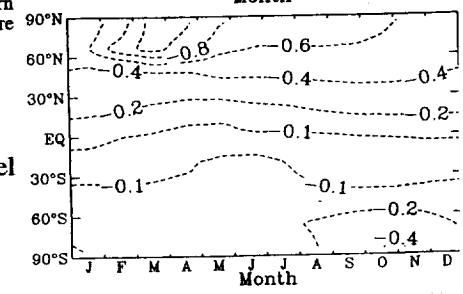

END TO END SENSITIVITY STUDIES

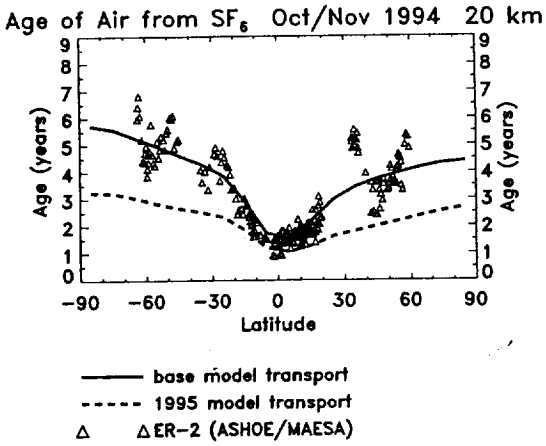

age from global avg at ground

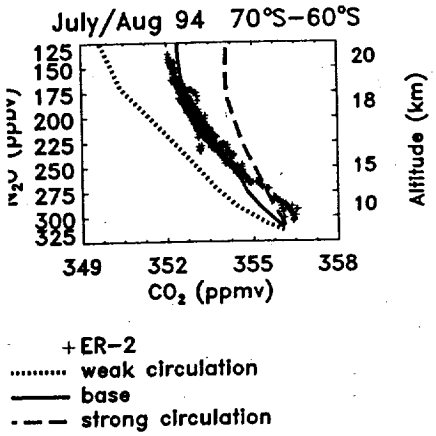

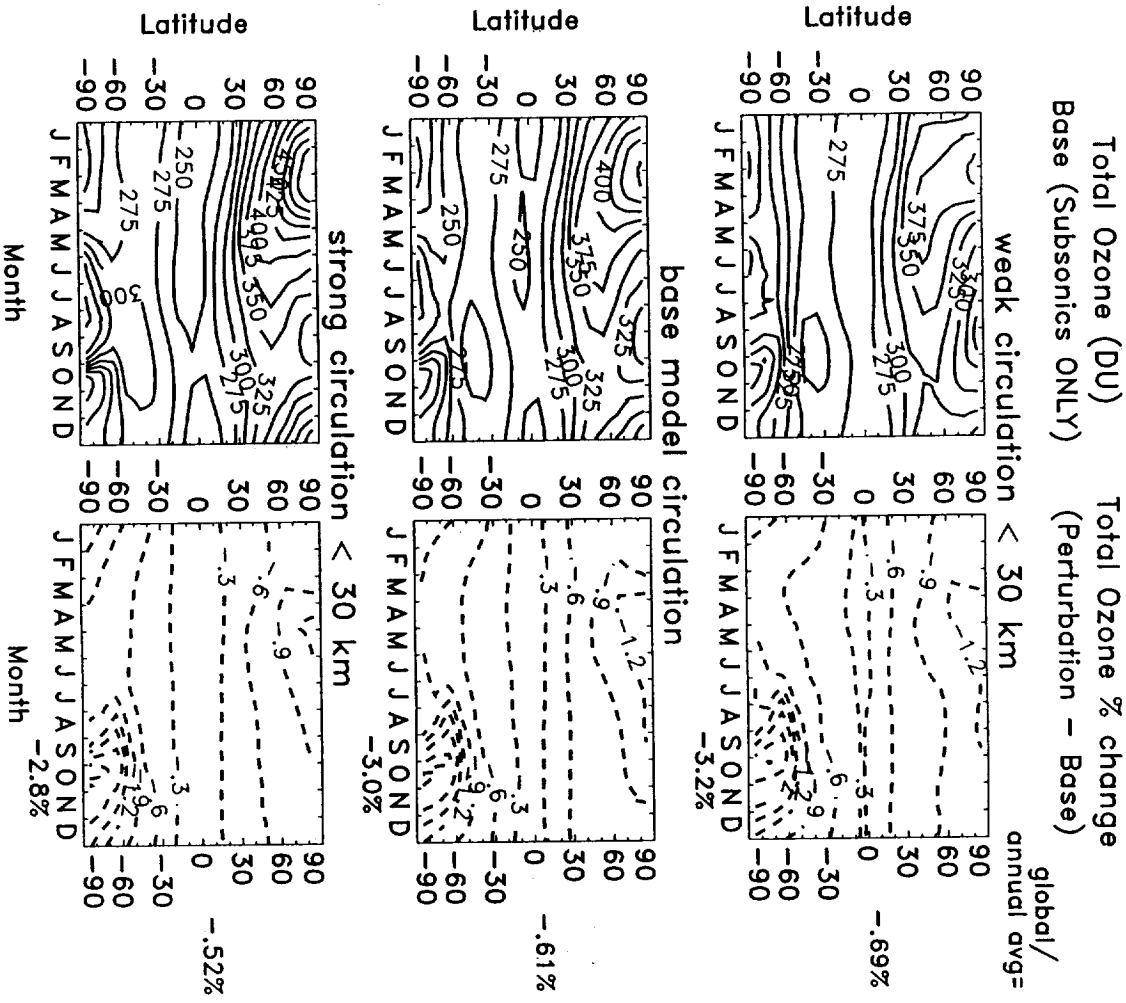

Other issues

- Long-term averaged (monthly) winds vs. "on-line" wind
- Interannual variabilities

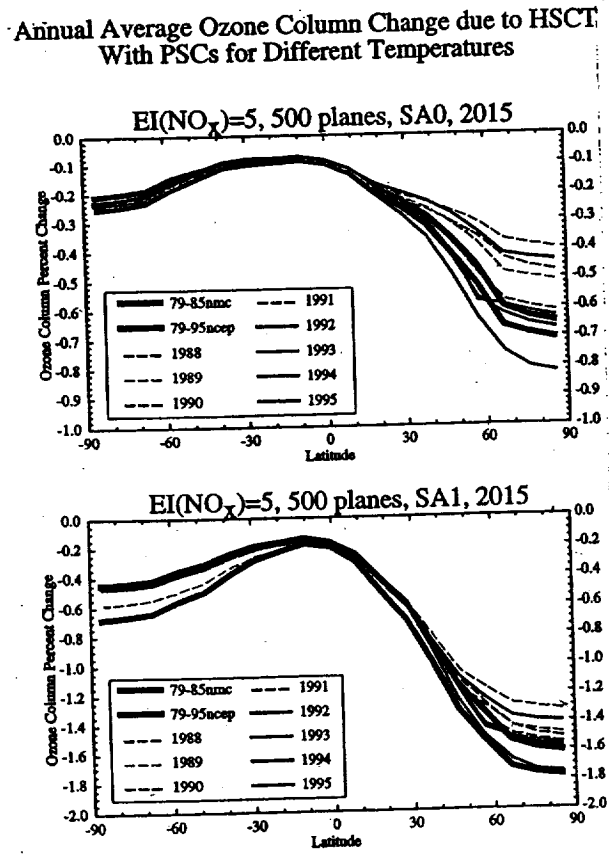

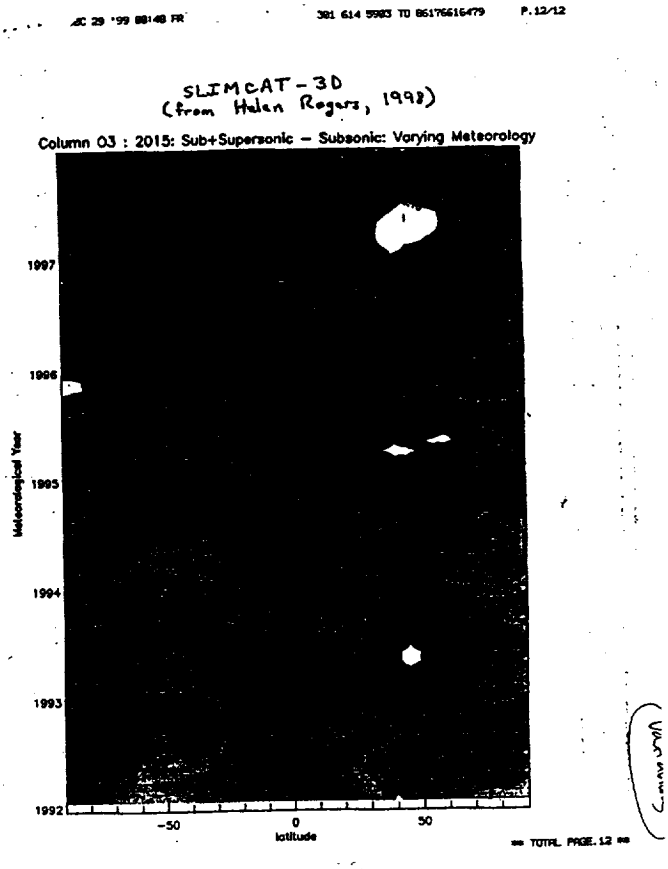

Appendix 5

Presentation at AESA Meeting

June 2000

Global Implications of the Ozone Loss in a Space Shuttle Wake

M.Y. DANILIN, M.K.W. KO, and D.K. WEISENSTEIN
AER, Inc., 840 Memorial Drive, Cambridge, MA 02139

Key Question:

How important is ozone loss in a Space Shuttle wake on the global scale?

AEAP Annual Meeting, Snowmass, CO, June 2000

Introduction

Space Shuttle emits 68 tons of chlorine per launch into the stratosphere.

In situ measurements [*Ross et al.*, 1997;2000] and model calculations [e.g., *Danilin*, 1993; *Zittel*, 1994] show a severe ozone depletion (up to 100%) in a Solid-fueled Rocket Motor (SRM) wake if emitted HCl is converted Cl_2 via afterburning processes.

Existing global model calculations [*Prather et al.*, 1990; *Jackman et al.*, 1996,1998] of the ozone response to SRM launches ignore ozone loss in the SRM wakes.

Is this assumption justified?

Addressing this question, we estimate the upper bound of the ozone depletion in the Space Shuttle wake and its implications on the global scale. To achive this goal, we assume that ALL chlorine is emitted as Cl_2.

Far-Wake Model

AER far-wake model [*Danilin et al.*, 1997] with updated reaction rates [*Sander et al.*, 2000] is used. The model assumes a uniform distribution of species across the wake and starts calculations 10 s after exhaust.

Wake Dilution Scenarios

$$R(z,t) = R(t_o) + b(t - t_0)(p(20km)/p(z))^{1/2}, \qquad (1)$$

b=1.75 m/s (baseline) and 7 m/s (fast), initial radius $R(t_o)$=200m, p(z) is the pressure at altitude z.

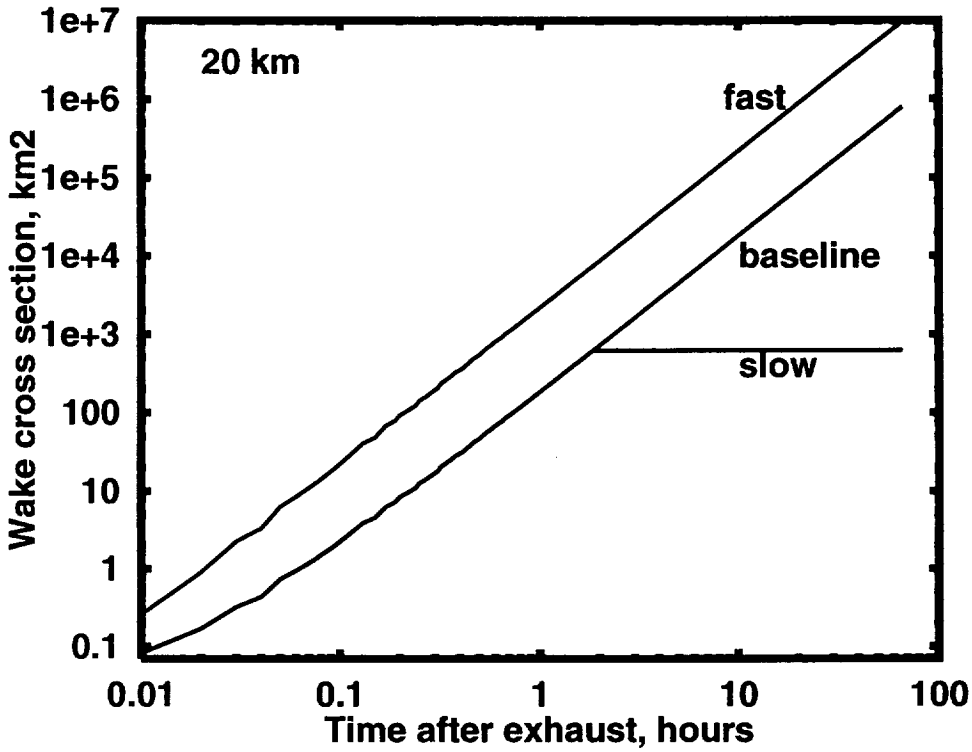

Mixing with Ambient Air

$$n_i(z, t + \delta t) = \frac{n_i(z,t)S(z,t) + n_i^a(z,t)\Delta S(z,t)}{S(z, t + \delta t)}, \qquad (2)$$

n_i(z,t) and n_i^a(z,t) are the concentrations of the i-th gas inside and outside the wake, S(z,t) is the wake cross section.

Model Initialization

The vertical profile of chlorine release from the Shuttle SRM according to *Whitten et al.* [1975] is used in this study. The main components of the Shuttle SRM are Al_2O_3 (30% by weight), CO (24%), chlorine(21%), H_2(10%), N_2(9%), CO_2(4%), and H_2 (2%) emitted up to 42 km [*Prather et al.*, 1990]. The Table below shows initial concentrations of Cl_2 in the wake with radius of 200 m. Initial concentrations of other exhaust products are obtained from the Cl_2 values by scaling: $n_i(z)=n_{cl2}(z)\times fr_i\times\mu_{cl2}/(fr_{cl2}\times\mu_i)$. Other species are taken from the AER 2-D model climatology at 29°N.

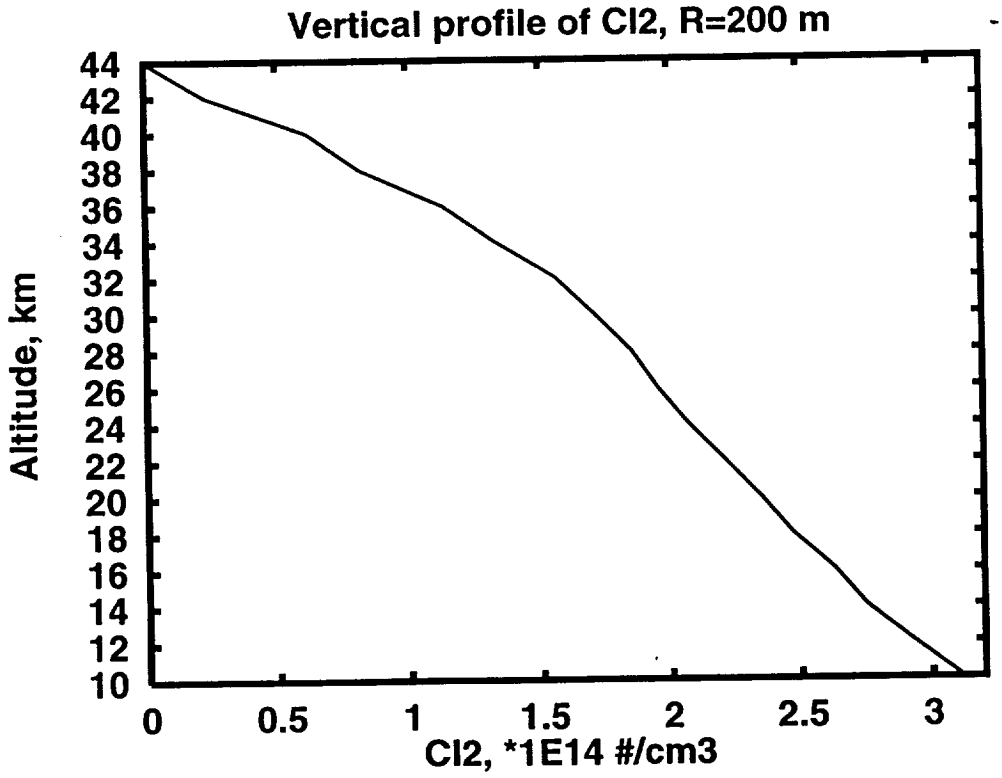

We split photochemical and wake dilution processes. The ozone responses shown are the difference between two runs: with and without Shuttle emissions.

Ozone response to chlorine emissions: HCl vs Cl_2

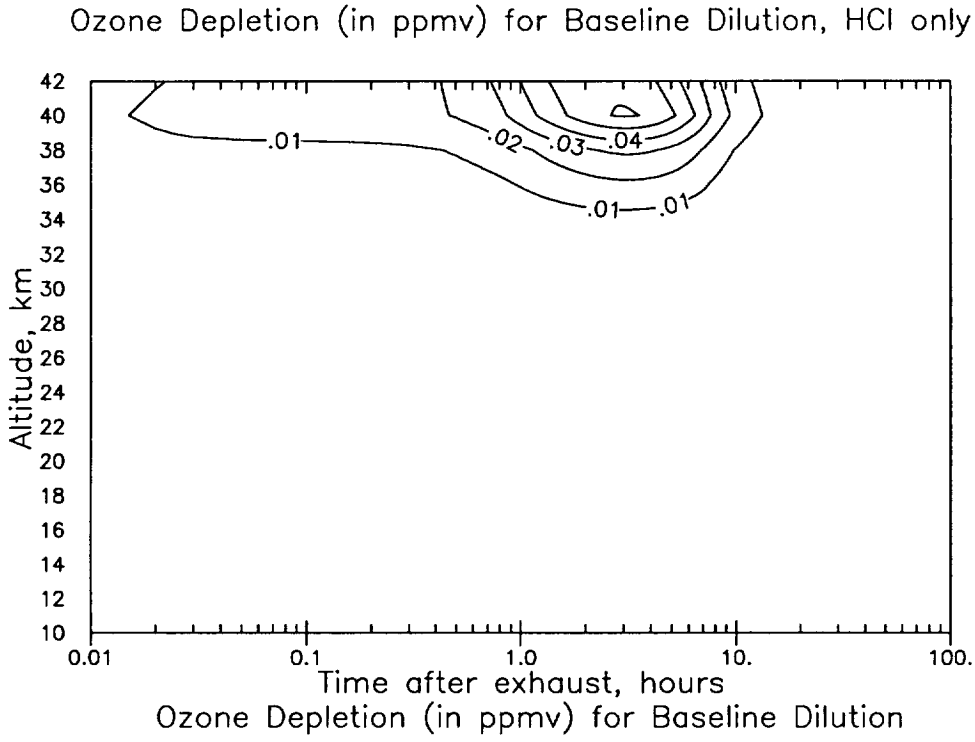

HCl

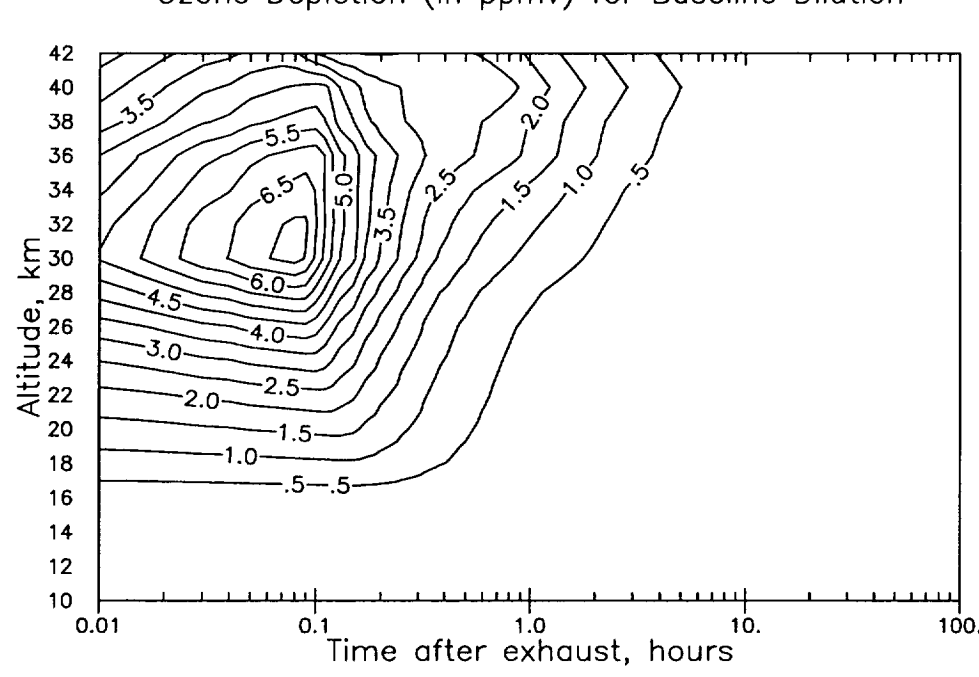

Cl_2

Ozone depletion in the wake is very sensitive to the form in which chlorine is released.

Baseline Case

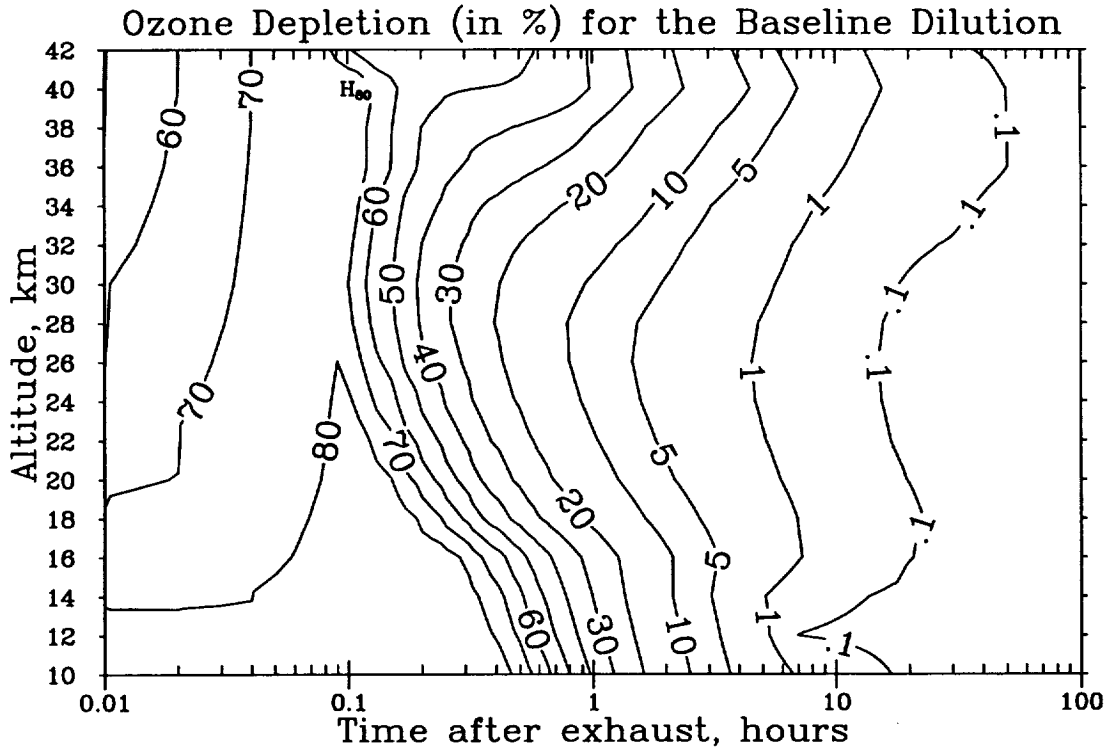

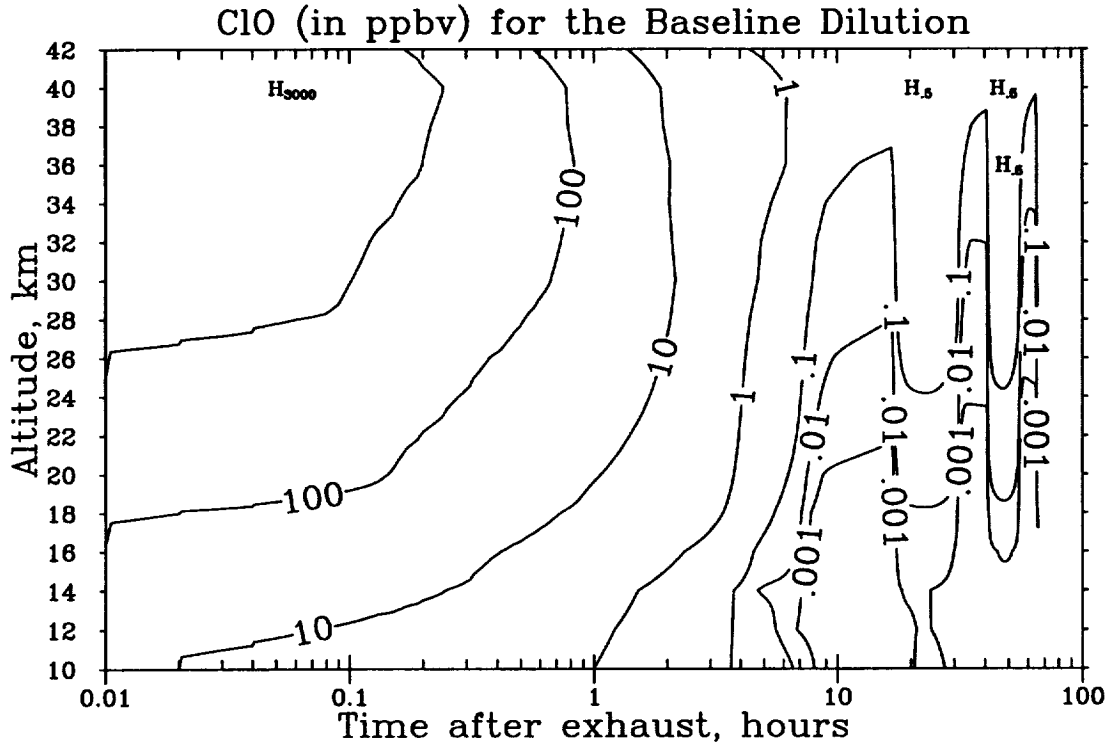

Ozone depletion (in % of its background values) and mixing ratios of ClO, Cl_2, and Cl_2O_2 (in ppbv) in the wake for a noon Shuttle launch in June.

Ozone Sensitivity to Wake Dilution Rate

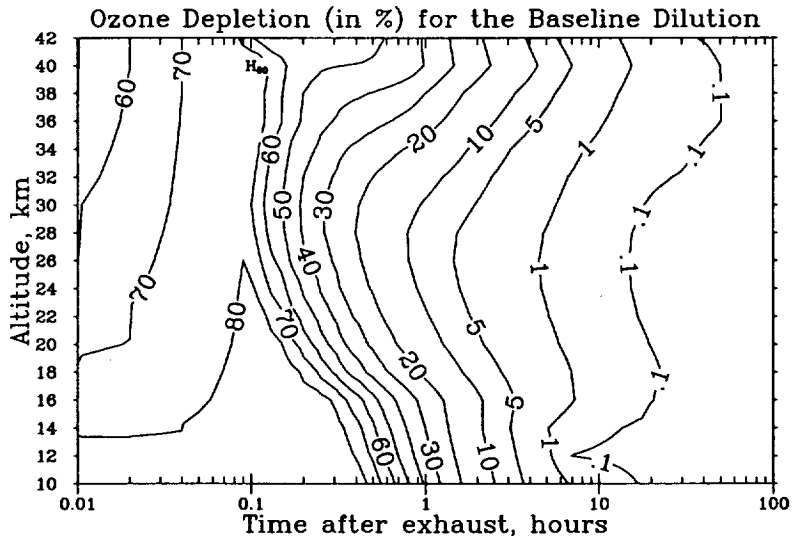

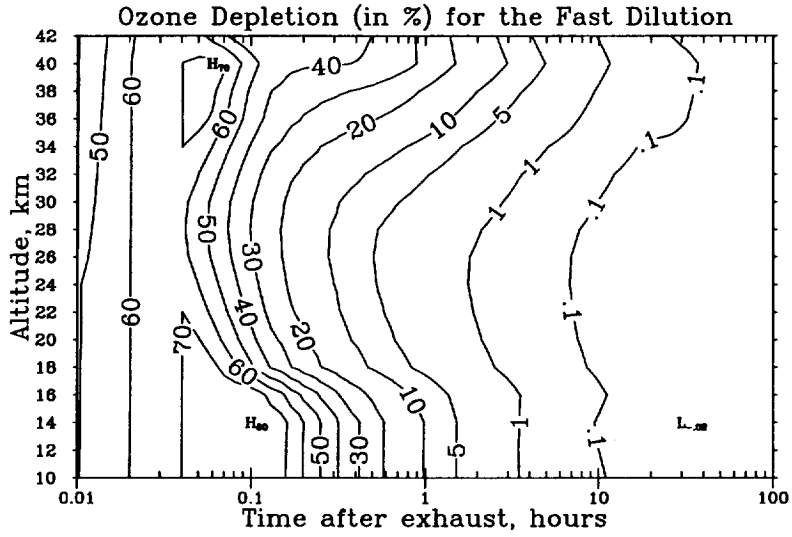

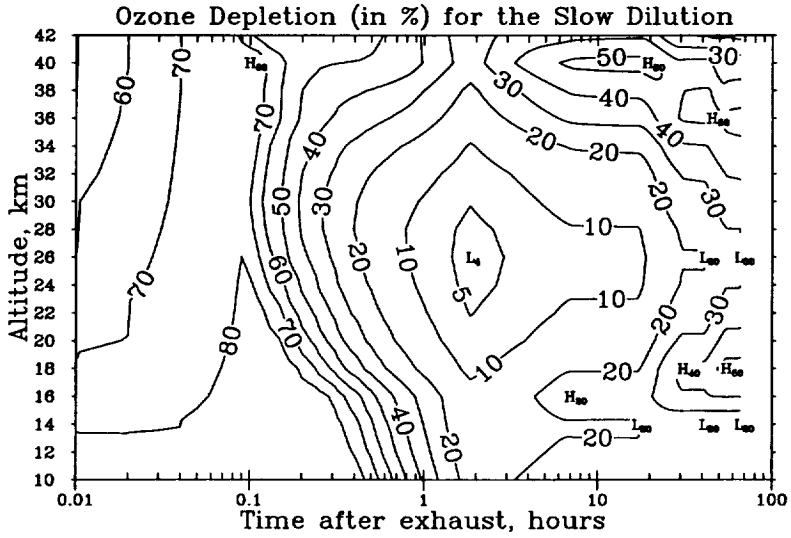

From the far-wake to global model

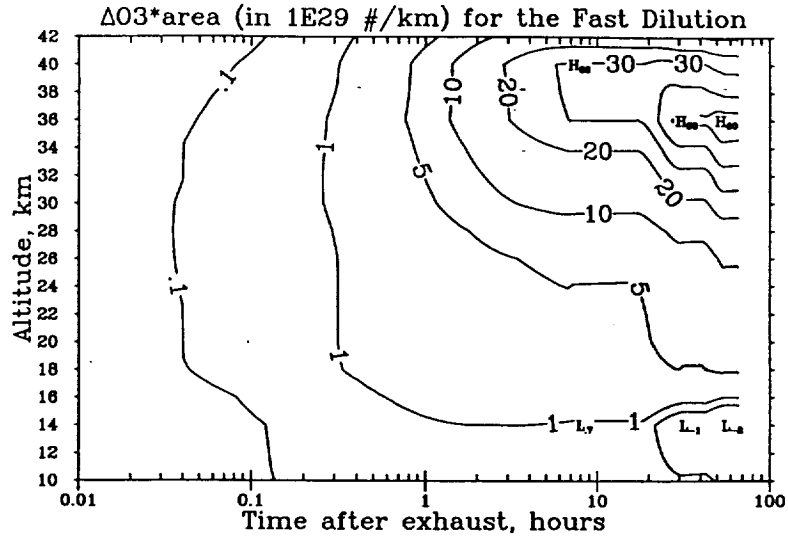

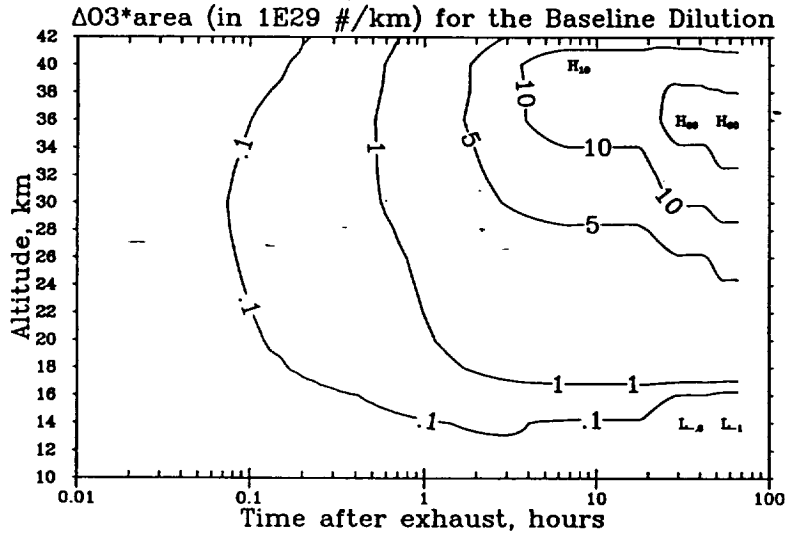

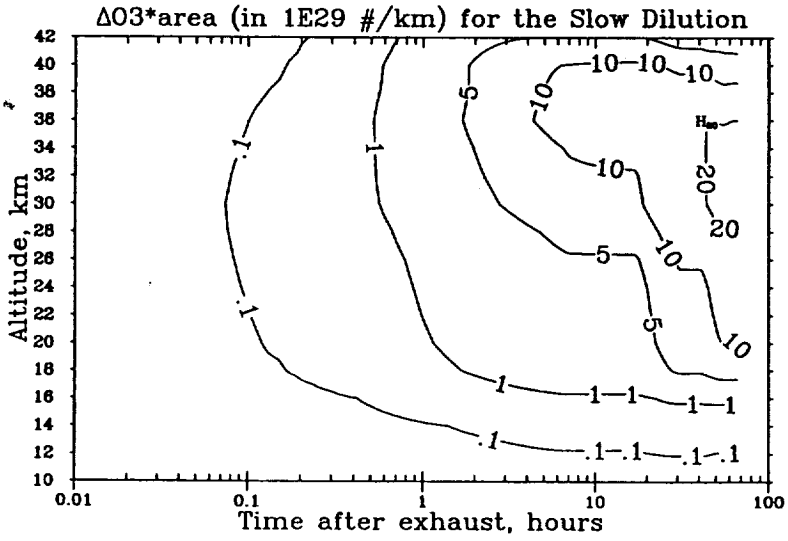

If $[\text{P-L}(O_3)]_{wake}$ and $[\text{P-L}(O_3)]_{ambient}$ are within $\pm 1\%$, the far-wake model results are ready for use in the AER 2-D model. We run the far-wake model 2 days to meet this criterion.

Theoretical estimates

Let consider a box where ozone has a photochemical lifetime τ and is periodically perturbed with amplitude ΔO_3^o and period T.

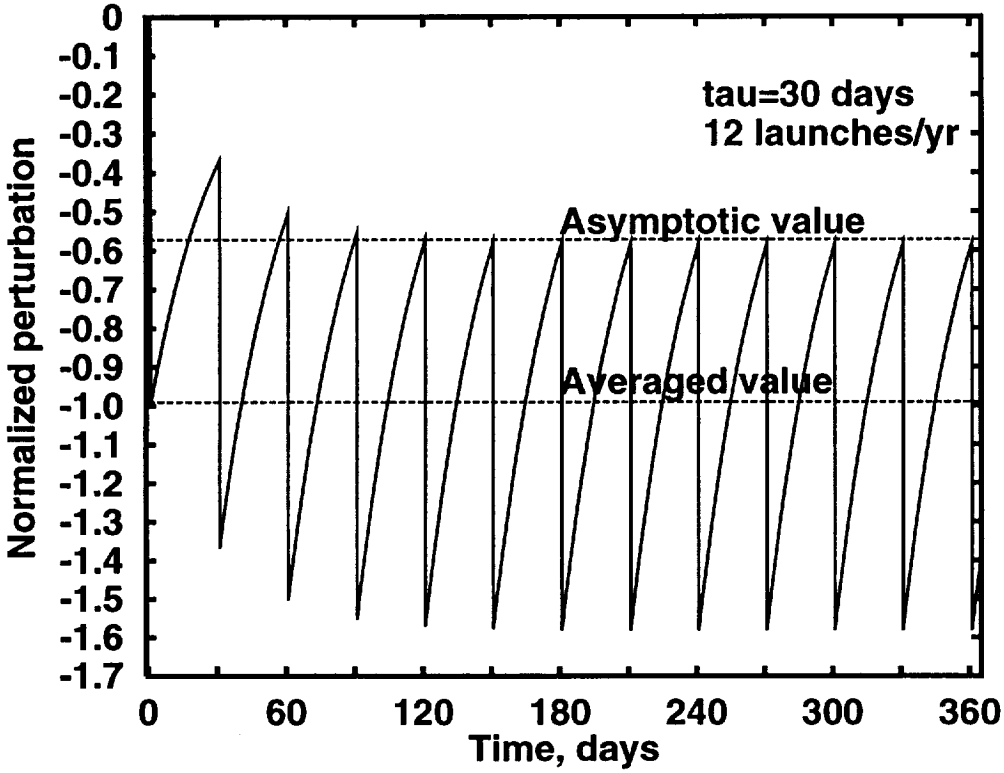

Asymptotic value

Definition: $\Delta O_3^{as} = (\Delta O_3^o + \Delta O_3^{as}) \times e^{-T/\tau}$

Solution: $\Delta O_3^{as} = \Delta O_3^o \times \frac{e^{-T/\tau}}{1-e^{-T/\tau}}$

Averaged value

Definition:

$$\Delta O_3^{av} = \frac{\Delta O_3^o + \Delta O_3^{as}}{T} \int_0^T e^{-t/\tau} dt = \Delta O_3^o \frac{\tau}{T}$$

Steady-state value

Definition: $\Delta O_3^{ss} = \Delta O_3^w(z, 2days) S^w(z, 2days) \Delta z \frac{\tau(z)}{T}$, T=365 days/12 launches

Estimates of the global effects of the wake ozone loss

Knowing ozone loss in the wake, wake size and photochemical lifetime of ozone from a global model, one can estimate global effects of the wake ozone depletion.

z, km	$\Delta O_3^w \times$VOL, $\times 10^{29}$	τ, days	ΔO_3^{ss}, $\times 10^{29}$
10	0.2	16.5	0.11
12	1.8	13.8	0.82
14	2.2	15.2	1.10
16	2.4	15.0	1.18
18	10.4	13.9	4.75
20	12.6	14.3	5.92
22	14.2	14.4	6.72
24	15.6	13.2	6.77
26	18.4	9.9	5.99
28	26.4	7.6	6.60
30	44.8	4.7	6.92
32	62.4	3.0	6.15
34	87.8	2.1	6.06
36	109.2	1.6	5.74
38	80.8	1.3	3.45
40	57.0	1.0	1.87
42	18.0	0.8	0.47
10-42	564.2	-	70.62

Peak value:

$$5.64 \times 10^{31}/(305 \times 2.687 \times 10^{26} \#/km^2 \times 3.71 \times 10^7 km^2) = 1.8 \times 10^{-3}\%$$

Steady-state value:

$$7.06 \times 10^{30}/(305 \times 2.687 \times 10^{26} \#/km^2 \times 3.71 \times 10^7 km^2) = 2.2 \times 10^{-4}\%$$

2-D Model Results

First run: 12 Shuttle launches per year from Cape Canaveral (29°N) inject 0.804 kt chlorine into the stratosphere;

Second run: Additionally, the wake ozone loss is simulated by removing $\Delta O_3^{2D}(z)$ (in #/km^3) between 10 and 42 km altitde in the 23°N-33°N band:

$$\Delta O_3^{2D}(z) = \Delta O_3^{w}(z, 2\text{days}) \frac{S^{w}(z, 2\text{days})}{S_{\text{grid}}^{2D}}$$

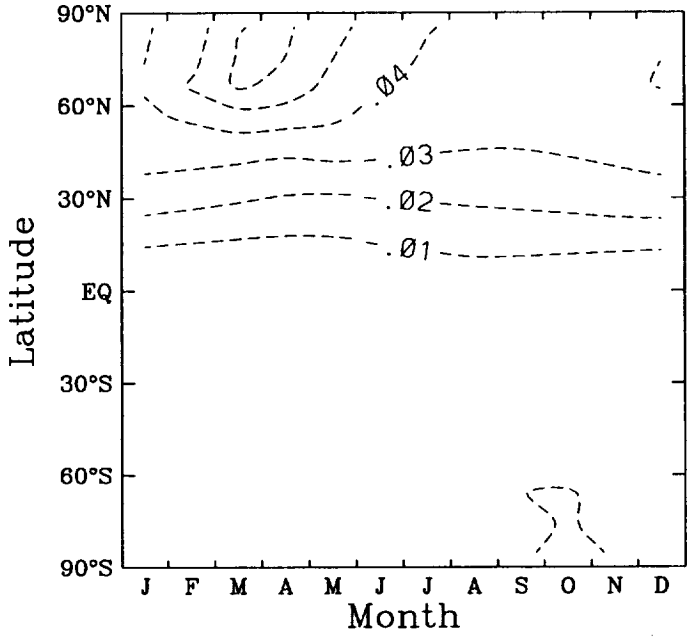

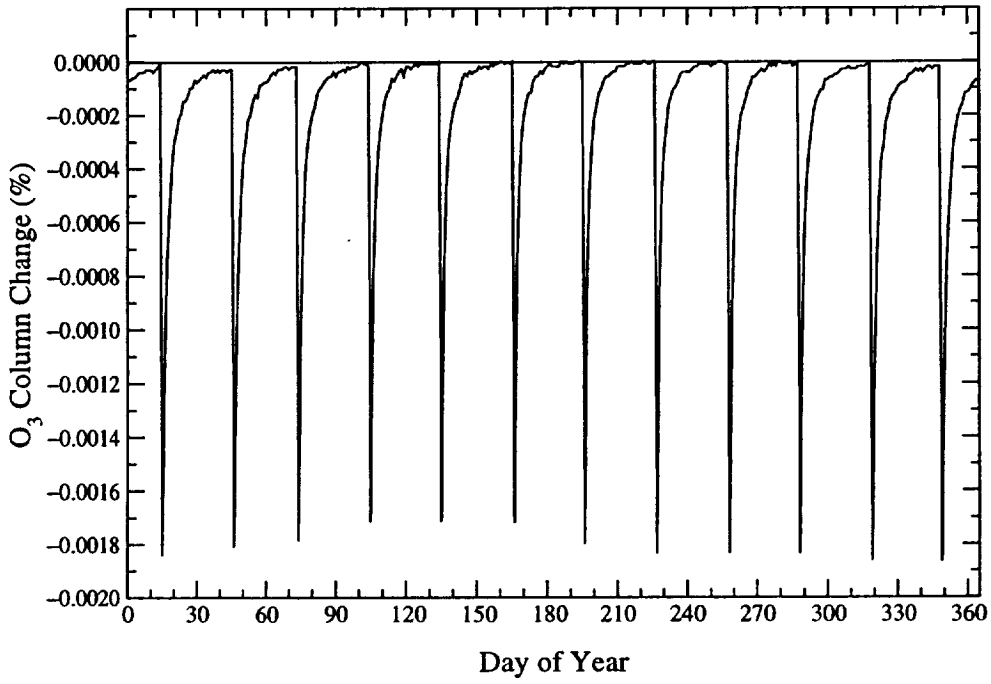

Ozone Impact: Shuttle vs Aircraft

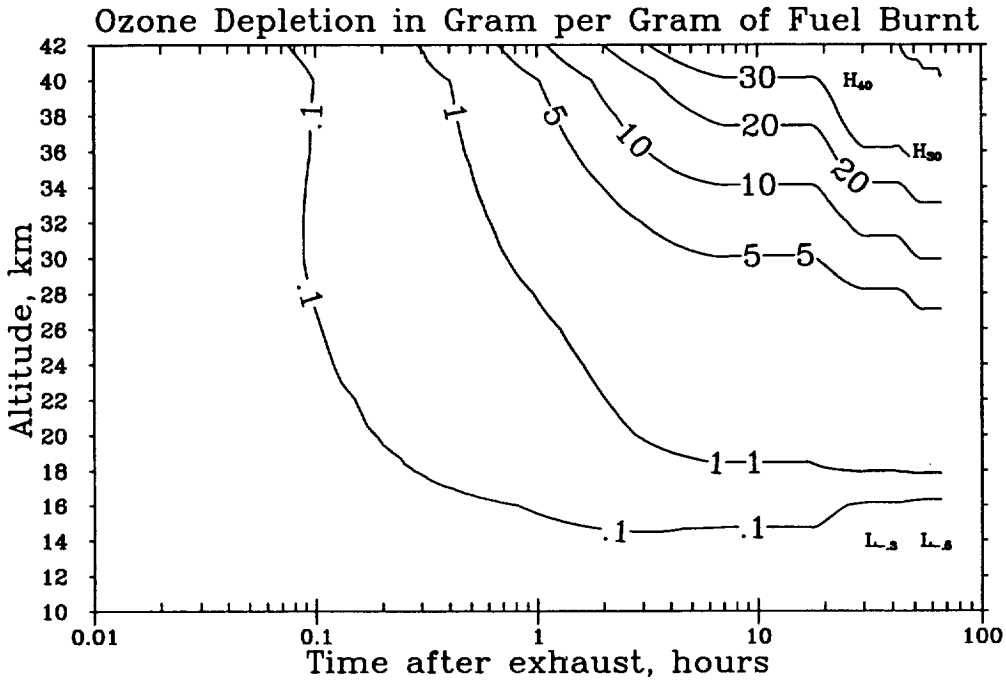

Shuttle: Effective Emission Index EEI = -(1-30) g(O_3)/g(fuel) 2 days after exhaust (upper bound!!!).

HSCT: assuming 1.1×10^9 #/cm^3 is depleted in the wake with volume of 1 km $\times$20 km^2 due to 8.9 kg of fuel burnt [*Danilin et al.*, 1997], one gets negative effective **EEI**=-1.1×10^{24} #/km$^3\times$20km$^3\times$48 g/mol/(6.02×10^{23} 1/mol $\times$ 8900 g) = **-0.2 g(O_3)/g(fuel)**, or **an order of magnitude smaller than in the Shuttle case at 20 km**.

Subsonic: Ozone production! ΔO_3=+0.02 ppbv [*Petry et al.*, 1998], wake volume =50 km^3, **EEI=+0.02 g(O_3)/kg(fuel)**

SUMMARY

- Upper bounds of the ozone loss in the Space Shuttle wake are estimated assuming all chlorine emissions are released as Cl_2;

- Local ozone depletion in the Space Shuttle wakes could reach 70-80% minutes after exhaust;

- Global effects of the ozone depletion in the wake are larger for faster wake dilution and summer sunrise launches of the Space Shuttle;

- Global effects of the ozone loss in the Shuttle wake are at least an order of magnitude less than that due to globally spread chlorine emissions from the Space Shuttle;

- $EEI(O_3)|_{shuttle} \approx 10 \times EEI(O_3)|_{hsct}$ at 20 km (caveats!)

Acknowledgement.
This study is supported by the NASA ACMAP and AEAP. We thank C.E. Kolb and M.N. Ross for discussions.